Θ^+ formation in inclusive $\gamma D \to pK^- X$

A. I. Titov,[1,2] B. Kämpfer,[3,4] S. Daté,[5] and Y. Ohashi[5]
[1]*RIKEN, 2-1 Hirosawa,Wako, Saitama 351-098, Japan,*
[2]*Bogoliubov Laboratory of Theoretical Physics, JINR, RU-141980 Dubna, Russia*
[3]*Forschungzentrum Rossendorf, D-01314 Dresden, Germany*
[4]*Institut für Theoretische Physik, TU Dresden, D-0162 Dresden, Germany*
[5]*Japan Synchrotron Radiation Research Institute, SPring-8, 1-1-1 Kouto Sayo-cho, Sayo-gun, Hyogo 679-5198, Japan*
(Received 27 July 2006; published 17 November 2006)

We analyze the possibility of producing an intermediate Θ^+ via a $KN \to \Theta^+$ formation process in $\gamma D \to pK^- X(X = nK^+, pK^0)$ reactions at some specific kinematical conditions, in which a pK^- pair is knocked out in the forward direction and its invariant mass is close to the mass of $\Lambda^*[\Lambda^* \equiv \Lambda(1520)]$. The Θ^+ signal may appear in the $[\gamma D, pK^-]$ missing mass distribution. The ratio of the signal (cross section at the Θ^+ peak position) to the smooth background processes varies from 0.7 to 2.5 depending on the spin and parity of Θ^+, and it decreases correspondingly if the pK^- invariant mass is outside of the Λ^*-resonance region. We analyze the recent CLAS search for the Θ^+ in the $\gamma D \to pK^- nK^+$ reaction and show that the conditions of this experiment greatly reduce the Θ^+ formation process making it difficult to extract a Θ^+ peak from the data.

DOI: 10.1103/PhysRevC.74.055206 PACS number(s): 14.20.−c, 13.85.Fb, 13.75.Jz

I. INTRODUCTION

The first evidence for the pentaquark hadron Θ^+, discovered by the LEPS Collaboration at SPring-8 [1], was subsequently confirmed in some other experiments [2]. However, many other experiments failed to find the Θ^+ signal (for surveys see Refs. [3–5]). Most of them came from the data analysis of high-statistics high-energy experiments. These null results at high energies were not so much surprising because it is natural to expect a sizable suppression in the production of the more complicated five-quark system compared to the conventional three-quark hyperons [6]. But the state of affairs became dramatic after the recent publication of the high statistics results of the CLAS Collaboration [7,8]. The first experiment is designed to search for the Θ^+ signal in $\gamma D \to pK^- nK^+$ in direct γn interactions at relatively low photon energy, $E_\gamma = 1.7-3.5$ GeV. The second one aimed to search for the Θ^+ signal in $\gamma p \to \bar{K}^0 nK^+$ and $\gamma p \to \bar{K}^0 pK^0$ reactions. Within the experimental significance, no Θ^+ signal was observed. Note, however, that recently the DIANA Collaboration confirmed a former result for Θ^+ production in K^+ interaction with Xe nuclei [9]. Another positive, but low statistics result on Θ^+ production in $\pi^- p$ interaction was obtained in KEK [10]. Therefore, the situation concerning the existence of the pentaquark state remains controversial.

Coming back to the high statistics CLAS experiments, one can conclude that if the Θ^+ exists, then the null result means that we do not understand the mechanism of Θ^+ photoproduction in elementary $\gamma N \to \Theta^+ \bar{K}$ reactions. Indeed, in all theoretical studies (for references, see the recent review article [11]) the cross section of this reaction is defined by the K and K^* exchange dynamics. In the first case, the amplitudes are proportional to the product of the Θ^+-nucleon-kaon coupling constant $g_{\Theta NK}$ and the form factor $F(p_\Theta^2, p^2, p_K^2)$, where p_B, p_K are the four-momenta of the baryon (nucleon or Θ^+) and the kaon, respectively. One of the hadrons is far off-shell. If one uses the $\Theta^+ \to NK$ decay width (Γ_Θ) as an input parameter, then the $g_{\Theta NK}$ coupling is fixed, but unfortunately, there are no guiding rules for the off-shell form factors that bring some ambiguity into the theoretical predictions. For K^* exchange processes the situation is even worse. In this case we do not know the $g_{\Theta NK^*}$ coupling constant (the ambiguity of its estimate is rather large [12]) and the "off-shellness" in the Θ^+- nucleon-K^* vertex is much greater because of the large mass difference between K^* and K mesons. The CLAS null result for a given finite Θ^+ decay width means large off-shell suppression of the amplitudes with $\Theta^+ NK$ vertices. The K^*-exchange amplitude may be additionally suppressed by the small value of the $g_{\Theta NK^*}$ coupling constant because it is not related directly to the Θ^+ decay width and therefore remains unconstraint. Therefore, the best way to check whether the Θ^+ exists is to study the $KN \to \Theta^+$ fusion reaction with a quasifree kaon and a nucleon in the initial state. In this case the $g_{\Theta NK}$ coupling is fixed (for given Γ_Θ), and there is no ambiguity with the off-shell form factor because all hadrons are on the mass shell. This situation may be realized in the reaction $\gamma D \to \Lambda^* \Theta^+ \to pK^- nK^+[\Lambda^* \equiv \Lambda(1520)]$ with the Θ^+ showing up as a peak in the nK^+ invariant mass distribution as shown in Ref. [13]. There are several conditions that can enhance this effect. First, the pK^- invariant mass must be close to the mass of Λ^*. In this case, the total amplitude is the coherent sum of two amplitudes with charged and neutral kaon exchange shown in Fig. 1. The dominance of the K^* meson exchange in Λ^* photoproduction [13–15] results in a constructive interference between the two amplitudes which enhances the Θ^+ signal.

Second, the deuteron wave function greatly suppresses the processes with a fast-moving recoil nucleon, therefore, the experiment must be able to measure an extremely slow-moving recoil (spectator) nucleon that participates in the $KN \to \Theta^+ \to KN$ reaction. And, third, the pK^- pair must be knocked out in the forward direction. In this case, the momentum of the recoil kaon is small, and it can merge with the slow-moving spectator nucleon to produce a Θ^+.

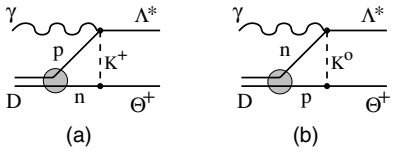

FIG. 1. Tree-level diagrams for the reaction $\gamma D \to \Lambda^* \Theta^+$. The exchange of charged and neutral kaons is shown in (a) and (b), respectively.

The CLAS experiment [7] to search for Θ^+ was designed to study the direct $\gamma n \to \Theta^+ K^- \to n K^+ K^-$ reaction and, in principle, it does not satisfy the above conditions. Thus, the Θ^+ and the outgoing neutron have finite momenta, and, therefore, the experiment has a neutron-momentum cut of $p_n > 0.2$ GeV/c. To reduce the contribution of K^- mesons coming from Λ^* excitation the data analysis makes a cut on the Λ^* mass, i.e., the pK^- invariant mass is outside the Λ^* mass. It has cuts for the kaon momenta, $p_K > 0.25$ (GeV/c) and cuts for the angles for positive and negative particles, $\theta_+ > 9^\circ$ and $\theta_- > 15^\circ$, respectively. All these experimental conditions (the pK^-invariant mass, momenta, and the angle cuts), whereas being quite acceptable for studying the $\gamma n \to \Theta^+ K^-$ reaction result in a large suppression of the $K + N \to \Theta^+$ formation process in the $\gamma D \to pK^- nK^+$ reaction and reduce the ratio of Θ^+ resonance contribution (signal) to background (noise): S/N.

To avoid the obvious difficulty in measuring the slowly moving recoil nucleon one has to analyze the $[\gamma D, pK^-]$ missing mass distribution [16]. In this case, all momenta allowed by the conservation laws participate in the process and, of course, the dominant contribution would come from slow-moving nucleons. As a result, the total cross section strongly increases. Unfortunately, in this case the background processes increase roughly by a factor of 2 compared to the exclusive $\gamma D \to pK^- nK^+$ reaction, because both the nK^+ and pK^0 final states now contribute. Nevertheless, even under this circumstance such experimental conditions can give a better chance to see the Θ^+ signal, in case it exists.

The aim of the present article is to extend the results of Ref. [13] for the inclusive reaction $\gamma D \to pK^- X$, where $X = nK^+, pK^0$, toward finding favorable kinematical conditions for a manifestation of the Θ^+ signal. We are going to show that this signal is independent of the mechanism of the elementary $\gamma N \to \Theta^+ \bar{K}$ reaction if the pK^- pair is produced in the forward hemisphere.

Our article is organized as follows. In Sec. II we consider the kinematics of a $2 \to 4$ reaction and define the observables. In Sec. III we briefly discuss the elementary $\gamma N \to NK\bar{K}$ reaction, which is used later for estimating the resonant effect and background. Section IV is devoted to a description of the associated $\Theta^+ \Lambda^*$ photoproduction in γD interactions, where we discuss the most favorable kinematics for the coherent effect and the dependence of the cross section on Θ^+ spin and parity. In Sec. V we discuss two dominant components of the nonresonant background: spectator and rescattering channels. In Sec. VI we present our main results and give a comparison of a possible Θ^+ signal for the inclusive reaction $\gamma D \to pK^- X$ with favorable kinematics and the exclusive reaction $\gamma D \to pK^- nK^+$ under the CLAS conditions. We show that in latter case the Θ^+ signal is weak due to the experimental conditions. The summary is given in Sec. VII. In Appendices A and B we show some details for the kinematics considered and the amplitudes of the elementary rescattering processes.

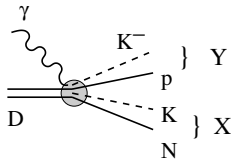

FIG. 2. Reaction $\gamma D \to pNK^-K$.

II. KINEMATICS

The differential cross section of the reaction $\gamma D \to pK^- X$, where $X = nK^+$ or pK^0, shown in Fig. 2, reads

$$\frac{d\sigma}{d[\cdots]} \equiv \frac{d\sigma}{dM_X dM_Y d\Omega d\Omega_X d\Omega_Y} = \frac{1}{64\pi^2 s_D} \frac{p_f}{p_i} \frac{1}{6} \sum_{NK,\lambda,m_D,m_p,m_N} \left|T_{\rm fi}^{NK}\right|^2 \frac{\tilde{q}}{16\pi^3} \frac{\tilde{\tilde{q}}}{16\pi^3}. \tag{1}$$

Hereafter, we use the following notations: X is the NK pair with mass M_X, Y is the pK^- pair with mass M_Y, p_f is the absolute value of the three-momentum of Y in the γD center-of-mass (c.m.) system, $p_i = |\mathbf{k}|$ is the absolute value of the photon momentum in the c.m. system, s_D denotes the square of the total energy in this system, $\tilde{q}$ and $\tilde{\tilde{q}}$ stand for the absolute values of the K and K^- mesons momenta in the rest frames of the X and Y systems, respectively. The indices m_D, m_p, m_N correspond to the spin projections of the deuteron, outgoing proton and nucleon, respectively, λ is the photon helicity; Ω_X and Ω_Y are the solid angles of the directions of flight of K and K^- mesons in the rest frames of the X and Y systems, respectively; Ω is the solid angle of the Y system in the c.m. system. The quantization axis $\mathbf{z}$ is chosen along the photon momentum, and the $\mathbf{y}$ axis is perpendicular to the production plane of X and Y pairs: $\mathbf{y} = \mathbf{z} \times \mathbf{p}_Y / |\mathbf{p}_Y|$, where $\mathbf{p}_Y$ is the three-momentum of the Y system in the c.m. system. $T_{\rm fi}^{NK}$ represents sum of the amplitudes of the resonant ($\gamma D \to \Theta^+ \Lambda^* \to pK^- X$), semiresonant ($\gamma D \to \Theta^+ pK^- \to pK^- X$), and nonresonant ($\gamma D \to pK^- X$) processes.

The invariant mass distribution $d\sigma/dM_X$ is defined as a six-dimensional integral

$$\frac{d\sigma}{dM_X} = 2\pi \int \frac{d\sigma}{d[\cdots]} dM_Y \, d\cos\theta \, d\Omega_X d\Omega_Y. \tag{2}$$

To define the four-momenta of all particles involved in the process appearing as arguments of the corresponding elementary amplitudes, we use the following incoming kinematical variables: photon four-momentum (laboratory system): $k_L = (E_L, 0, 0, E_L)$; deuteron four-momentum (laboratory system): $p_D = (M_D, 0, 0, 0)$; invariant masses M_X and M_Y; the polar

angle of pK^- pair photoproduction in the c.m. system θ; and the solid angles Ω_X and Ω_Y.

Using these variables we now calculate all momenta in the γD c.m. system (for details see Appendix A) and then transform them to the laboratory system. That is because the deuteron wave function is well defined only in the laboratory system.

In our study we analyze the missing mass distribution in the range $M_{\min} < M_X < M_{\max}$, where $M_{\min} = M_N + M_K$ and $M_{\max} = \sqrt{s_D} - M_N - M_K$ in several selected regions of the invariant mass $M_Y = M_0 \pm 20$ MeV, where M_0 is the mean value of the selected region of the pK^- invariant mass. The $KN \to \Theta^+$ transition leads to a Θ^+ signal in the missing mass distribution. Associated $\Lambda^*\,\Theta^+$ photoproduction manifests itself most clearly for $M_0 = M_{\Lambda^*}$ and $M_X \sim M_{\Theta^+}$. The coherent signal must be suppressed outside of the resonance position. To analyze this situation we choose M_0 at the resonance position with $M_0 = M_{\Lambda^*}$ and at a larger value ($M_0 = 1.62$ GeV). We also analyze the sensitivity of the Θ^+ signal to the pK^- pair photoproduction angle to get a maximum value for the S/N ratio. This gives the conditions for the range of integration over θ. In Eq. (2) integration over $\Omega_{X(Y)}$ is performed in all regions. In case of the CLAS conditions we do the integration over the available pK^- invariant mass distribution with taking into account specific data analysis conditions (see Sec. VI B).

III. ELEMENTARY $\gamma N \to N\bar{K}K$ REACTION

The mechanism of $\bar{K}K$ photoproduction in γN interaction is quite complicated because many processes can contribute. In our consideration we select the channel with an intermediate excitation of Λ^*, $\gamma N \to \Lambda^* K \to N\bar{K}K$, and denote it hereafter as the"resonant" channel. As we demonstrate, this process is dominant in the associated $\Lambda^*\Theta^+$ photoproduction at $E_\gamma \sim 2$ GeV.

We denote all other channels as "nonresonant" background. Of course, this notation is rather conventional, because the $\bar{K}K$ pairs can also be produced from the virtual vector mesons, hyperon resonances other than Λ^*, and so on. In this case the notation resonant indicates that only the Λ^* resonance excitation is selected. In this work we do not put emphasis on Θ^+ photoproduction in γN interactions because, at the considered kinematics when pK^- is produced in the forward direction with a fast moving proton, this channel is strongly suppressed by the deuteron wave function. Indeed, a sizable contribution of the associated $\Theta^+ pK^-$ photoproduction with $\gamma N \to \Theta^+ \bar{K}$ and $\bar{K} N_s \to pK^-$ subprocesses at fixed pK^- invariant mass is expected in case of a slowly moving spectator nucleon (N_s) and recoil intermediate antikaon. This situation is realized for forward Θ^+ photoproduction (with respect to the photon momentum) and backward photoproduction of the pK^- pair, respectively, which is not considered in present article.

In this section all variables are given in the γN c.m. system.

A. Reaction $\gamma N \to \Lambda^* K \to N\bar{K}K$

In this part we follow closely our previous article [13] and recall the main aspects of our considerations for the sake of completeness. We assume, that at low photon energies, close to threshold, the amplitude of Λ^* excitation in the $\gamma N \to N\bar{K}K$ reaction may be described by the effective Lagrangian formalism, whereas at high energies, the Regge model with the K^* exchange as a leading trajectory can be used. The value $E_\gamma = 2.3$ GeV is chosen as the matching point between these two regimes.

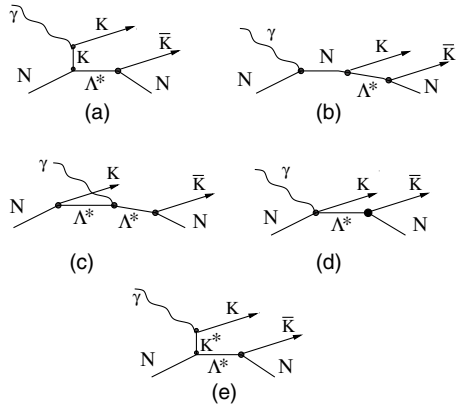

FIG. 3. Tree-level diagrams for the reaction $\gamma N \to \Lambda^* K \to N K \bar{K}$.

The tree-level diagrams for $\gamma N \to \Lambda^* K$ reaction at low energies are shown in Fig. 3. Figures 3(a)–3(d) correspond to the t, s, and u exchange amplitudes and the contact term, respectively, and are denoted as the Born terms. Figure 3(e) describes the t-channel K^* exchange amplitude. We neglect the photon interaction within the decay vertex and restore the gauge invariance by a proper choice of the contact term.

The amplitudes of the $\gamma p \to \Lambda^* K^+$ and $\gamma n \to \Lambda^* K^0$ reactions at low energy read

$$A^{\Lambda^*}{}_{\rm fi}(\gamma p) = \bar{u}^{\sigma}_{\Lambda^*}(p^*_\Lambda)\big[\mathcal{M}^s{}_{\sigma\mu} + \mathcal{M}^t{}_{\sigma\mu} + \mathcal{M}^c{}_{\sigma\mu} + \mathcal{M}^t{}_{\sigma\mu}(K^*)\big]u_p(p)\,\varepsilon^\mu, \quad (3a)$$

$$A^{\Lambda^*}{}_{\rm fi}(\gamma n) = \bar{u}^{\sigma}_{\Lambda^*}(p^*_\Lambda)\big[\mathcal{M}^s{}_{\sigma\mu} + \mathcal{M}^t{}_{\sigma\mu}(K^*)\big]u_n(p)\varepsilon^\mu, \quad (3b)$$

where u_{Λ^*}, u_N are the Λ^* and nucleon spinors, respectively, and ε^μ is the photon polarization vector. At high energy ($E_\gamma > 2.3$ GeV) they are replaced by the t-channel K^* meson exchange amplitude with Reggeized K^* meson propagator. The explicit form of the transition operators $\mathcal{M}^i_{\sigma\mu}$ as well as the choice of parameters are given in Ref. [13].

The total cross section of the reaction $\gamma p \to \Lambda^* K^+$ as a function of the photon energy from Ref. [13] together with available experimental data [14] is exhibited in Fig. 4. Similar results are obtained in Refs. [15,17] using slightly different approaches.

Figure 5 shows the differential cross sections for $\gamma p \to \Lambda^* K^+$ and $\gamma n \to \Lambda^* K^0$ as a function of the kaon production angle in the γN c.m. system at different E_γ in the near-threshold region. The difference in shape for these two reactions at forward photoproduction angles is explained by the sizable contribution of the Born amplitudes in the γp reaction. In the γn reaction the Born term (s-channel) is small, and the main contribution comes from the K^* exchange process. At backward photoproduction the shapes and the absolute values of the cross sections for γp and γn are similar

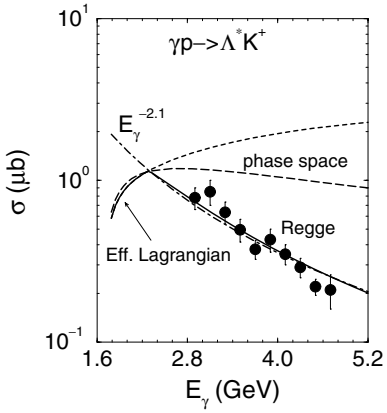

FIG. 4. The total cross section of the reaction $\gamma p \to \Lambda^* K^+$ as a function of the photon energy. The experimental data are taken from Ref. [14]. The dot-dashed curve is a fit to this data by $\sigma \simeq 0.7(\mu\text{b})\,[2.9(\text{GeV})/E_\gamma]^{2.1}$. The long-dashed curve represents the cross section for a constant amplitude $|T_0| = 5.95\ \text{GeV}^{-1}$ (see discussion above Eq. (4) below). The solid curve corresponds to a solution in the low- and high-energy regimes. The dashed curve describes the extrapolation of the effective Lagrangian model to the high energy region. See Ref. [13] for more details.

to each other, but the total cross sections for γp is larger. At $E_\gamma = 1.8$–2.3 GeV it varies from 0.59 to 1.14μb as compared with 0.27 to 1.08μb for γn.

As shown in the next section, the dominant contribution to the associated $\Lambda^*\Theta^+$ photoproduction comes from the backward angle of the K photoproduction in the $\gamma N \to \Lambda^* K$ reaction. In Fig. 6 we show the differential cross section at $E_\gamma = 2.1$ and 3.8 GeV together with available experimental data [14]. One can see that for increasing initial photon energy the cross section decreases at backward angles for the K photoproduction. Therefore, we expect that the threshold region with $E_\gamma \leqslant 2.1$–2.2 GeV is most favorable for studying associated $\Lambda^*\Theta^+$ photoproduction that reflects the Θ^+ formation.

We stress some ambiguity in the choice of the matching point $E_\gamma = 2.3$ GeV, which will be eliminated after measuring the $\Lambda(1520)$ photoproduction cross section at low energy with $E_\gamma = 1.7$–3 GeV. However, we believe that the present model can still be used for our aim. First, it gives reasonable energy dependence of the cross section: some increase just near

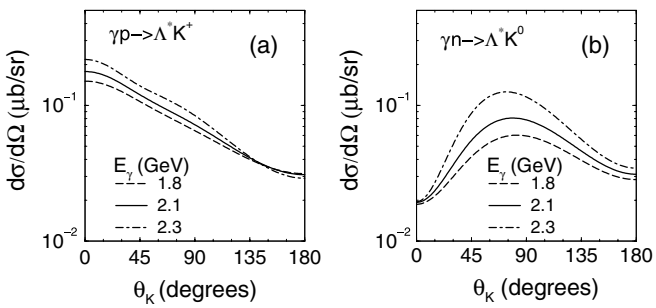

FIG. 5. The differential cross section of the reactions $\gamma p \to \Lambda^* K^+$ (a) and $\gamma n \to \Lambda^* K^0$ (b) as a function of the kaon photoproduction angle in γN c.m. system at $E_\gamma = 1.8$, 2.1, and 2.3 GeV.

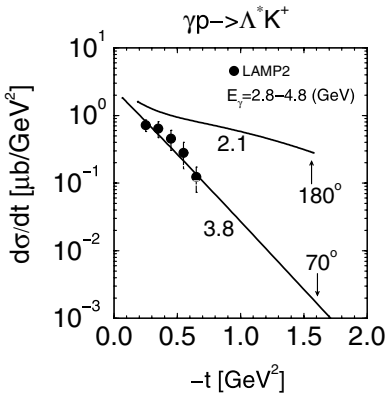

FIG. 6. The differential cross section for the $\gamma p \to \Lambda^* K^+ E_\gamma = 2.1$ and 3.8 GeV. Experimental data from Ref. [14].

the threshold (explained mainly by the phase-space factor) and then some decrease, usual for the inelastic processes, confirmed by other authors using different approaches (see Refs. [15,17]). Second, and most important: in case of low energy both the Θ^+ formation cross section and the background dominated by the quasifree Λ^* photoproduction are described by the same elementary amplitudes, Eqs. (3a) and (3b). Therefore the signal-to-noise ratio, which is main goal of our study, is not sensitive to the details of Λ^* photoproduction.

Finally, let us mention that in our approach the total sign of the Λ^* photoproduction amplitude follows the sign of the K^* exchange amplitude. Thus, in the γp reaction the interference between K^* exchange and Born terms is constructive, i.e., their total sign coincide with the sign of the K^* exchange amplitude. In the γn reaction the K^* exchange is the dominant channel. But SU(3) symmetry predicts opposite signs for the $\gamma K^{*-} K^+$ and $\gamma \bar{K}^{*0} K^0$ couplings, which results in opposite signs of the total amplitudes in γp and γn reactions.

B. Nonresonant $\gamma N \to N\bar{K}K$ reactions

In Ref. [13] we assumed that the dominant contribution to the nonresonant $\gamma p \to p K^+ K^-$ reaction comes from the virtual vector-meson production ($\gamma p \to pV \to p K^+ K^-$) and intermediate $\Lambda(1405)$ excitation [$\gamma p \to \Lambda(1405) K^+ \to p K^+ K^-$]. We believe that the vector-meson contribution is under control because the mechanism of real vector-meson photoproduction is well known. As an example, in Fig. 7 we show the differential cross sections for ϕ meson photoproduction at $E_\gamma \sim 2$–3 GeV calculated using the model of Ref. [18] together with the available experimental data. One can see that the description of this reaction is quite reasonable. Next, the coupling constant of $\phi K^+ K^-$ can be extracted from the $\phi \to K^+ K^-$ decay, and the $\rho K^+ K^-$ and $\omega K^+ K^-$ couplings can be found from SU(3) symmetry relations. Then, the contribution to $K^+ K^-$ photoproduction from the virtual vector-meson excitation may be easily evaluated. But at this moment, we have to make two comments. First, in the $\gamma N \to N\bar{K}K$ reaction the virtual vector mesons are off mass shell and, therefore, one has to introduce the corresponding form

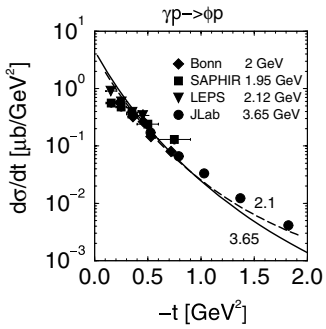

FIG. 7. The differential cross section of ϕ meson photoproduction based on the model of Ref. [18]. Data from Refs. [19–22].

factors [18]. The form factors, together with the vector-meson propagators, strongly suppress contributions of the virtual ρ and ω mesons, leaving only a noticeable contribution from the ϕ meson, which is almost on-shell because of the small decay width of the ϕ meson. Second, in the data analysis for Θ^+ photoproduction the contribution of the ϕ meson can be excluded by making a corresponding "ϕ-meson cut" [1,7]. Nevertheless, we discuss it here to fix other sources of K^+K^- photoproduction, having in hand only the total cross section $\sigma^{K^+K^-}$ of the $\gamma p \to pK^+K^-$ reaction [23].

The situation with the contribution from the $\Lambda(1405)$ is not so transparent. At $E_\gamma = 1.8$–2.5 GeV, there is some difference ($\Delta\sigma^{K^+K^-}$) on the level of 10–30% between the total cross section $\sigma^{K^+K^-}$ and the total contribution from Λ^* and vector-meson excitations. This difference increases at higher energies, because $\sigma^{K^+K^-}$ increases with energy, whereas the contribution from Λ^* decreases with energy and the contribution from the ϕ mesons stays constant. At low energies, $\Delta\sigma^{K^+K^-}$ may be identified with the virtual excitation and decay of hyperons other than Λ^*. Thus, for example, Oh, Nakayama, and Lee considered contributions from $\Lambda(1405)$, $\Lambda(1116)$, $\Sigma(1193)$, and $\Sigma(1385)$ [11]; and Roberts included additionally contributions from $\Lambda(1600)$, $\Lambda(1670)$, $\Lambda(1690)$, $\Lambda(1800)$, $\Lambda(1810)$, $\Lambda(1890)$ and $\Sigma(1620)$, $\Sigma(1660)$, $\Sigma(1670)$, $\Sigma(1730)$, $\Sigma(1880)$, $\Sigma(1940)$ [24]. In principle, one can also add contributions from $\Sigma(1480)$ and $\Sigma(1560)$ hyperons, listed in PDG [25].

Another source of $\bar{K}K$ pair photoproduction in γN reaction is the so-called Drell process [11,15,24], where the incoming photon virtually decays into a K^+K^- pair with subsequent quasielastic or charge-exchange KN rescattering. Also a $\bar{K}K$ pair may be produced from the virtual decay $\gamma \to KK^*$ with a subsequent inelastic $K^*N \to KN$ transition. It is quite clear that a consistent description of all the listed background sources is well beyond the present state-of-the-art because one needs a fairly large number of poorly known strength parameters, form factors, phases, and so on. Moreover, we need a proper description of the high-energy behavior of these processes. However, in case of a large number of background sources we can assume random relative phases between them that leads to cancellations of the interference terms. Also, as a first approximation one can choose the incoherent sum of the squares of the amplitudes to be a constant. This means that the energy dependence at low energies of this source of K^+K^- pairs is defined essentially by the phase-space factor. Our analysis of the Λ^* photoproduction shows that this approximation works well (see the solid and long dashed curves in Fig. 4 at low energy). The value of the constant matrix element can be obtained from a comparison with experimental data for the $\gamma p \to pK^+K^-$ reaction. In our further analysis we parameterize the amplitude of the additional contribution $\Delta\sigma^{K^+K^-}$ (for the sake of a concise notation, we denote it as BG_γ) by the constant matrix element with $|T_{BG_\gamma}| \equiv T_0 = 5.95\ \mathrm{GeV}^{-1}$. This parametrization, being quite reasonable at low energy with $E_\gamma \lesssim 2.3$ GeV, results in a somewhat larger rise of the cross section and overestimates the data by 20-50% at $E_\gamma = 3$–6 GeV. To fit the data, we multiply T_0 by a correction factor $C(E_\gamma)$

$$
\begin{aligned}
C^2(E) &= \theta(E_0 - E) + \frac{I_C(E_0)}{I_C(E)} \left(\frac{E}{E_0}\right)^{1.2} \theta(E - E_0), \\
I_C(E) &= \frac{1}{s\left(s - M_N^2\right)} \\
&\quad \times \int_{M_N + M_K}^{\sqrt{s} - M_K} \sqrt{\lambda\left(s, M^2, M_K^2\right) \lambda\left(M^2, M_N^2, M_K^2\right)}\, \frac{dM}{M}, \\
s &= M_N^2 + 2M_N E,
\end{aligned}
\tag{4}
$$

with the matching point $E_0 = 2.3$ GeV. In Fig. 8 we show the total cross section of the $\gamma p \to pK^+K^-$ reaction together with available experimental data [23].

To summarize this section we conclude that, for the elementary $\gamma p \to pK^+K^-$ process, which is used in our analysis of the $\gamma D \to pK^-X$ reaction, we have selected and described explicitly the Λ^* and vector-meson (ϕ meson) excitation channels. The sum of all other possible processes is parameterized effectively by a constant matrix element. The energy dependence of this channel follows the phase space. At higher energies, $E_\gamma = 2.3$–3.5 GeV, this dependence is slightly corrected. In case of $\gamma n \to pK^-K^0$, the vector meson may contribute only through virtual excitation of the ρ^- meson, which is negligibly small. For $\gamma n \to pK^-K^0$ channel we use the contribution from a Λ^* excitation in the γn reaction

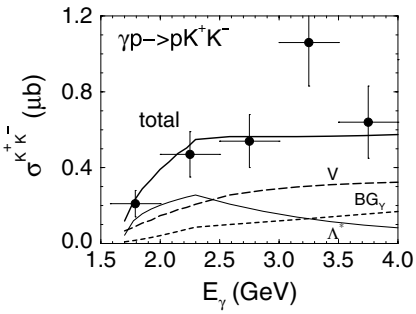

FIG. 8. The total cross section of the $\gamma p \to pK^+K^-$ reaction as a function of the photon energy. Thin solid curve is the contribution of Λ^* excitation, the dashed curve depicts the contribution of the vector-meson decay, all other sources denoted as BG_γ are shown by the short-dashed curve. The solid curve is the sum of all processes. Experimental data from Ref. [23].

and the contribution from nonresonant channels BG_Y, taking the same as for the γp reaction.

IV. ASSOCIATED $\Lambda^*\Theta^+$ PHOTOPRODUCTION

Now we turn to the associated $\Lambda^*\,\Theta^+$ photoproduction off the deuteron. Basically, our consideration of $\gamma D \to \Theta^+\Lambda^*$ is similar to that in Ref. [13]; however, we make several modifications. Therefore, for completeness, we recall the main aspects of our model to fix the new points. We assume that main contribution comes from the charged and neutral K meson exchange, shown in Figs. 1(a) and 1(b), respectively, and we do not discuss the diagrams with direct Θ^+ photoproduction being important at backward angles of pK^- pair photoproduction. In calculating the $K + N \to \Theta^+$ vertices we consider the Θ^+ decay width as an input parameter, taking $\Gamma_\Theta = 1$ MeV [26].

The amplitudes of the associated $\Lambda^*\Theta^+$ photoproduction are expressed through the transition operators of the "elementary" process $\gamma N \to \Lambda^* K$ as

$$A_{(a,b)} = g_{\Theta NK}\int \frac{d^4p}{(2\pi)^4}\,\bar u_\Theta\gamma_5\frac{1}{q^2-M_K^2}\,\bar u^\sigma_{\Lambda^*}\mathcal{M}^{\Lambda^*}_{\sigma\mu}\epsilon^\mu \times\frac{\not p + M}{p^2-M^2}\Gamma_D\frac{\not p' + M}{p'^2-M^2}U_D, \tag{5}$$

where the transition operator $\mathcal{M}$ defines the amplitude of Λ^* photoproduction and uses the sum of transition operators in Eqs. (3a) and (b); Γ_D and U_D stand for the deuteron np coupling vertex and the deuteron spinor, respectively; $p' = p_D - p$; and q is the momentum of the exchanged kaon. We begin our consideration for the case of Θ^+ spin-parity $\frac{1}{2}^+$. Generalization and discussion of our results for another Θ^+ spin-parity is relegated to the end of this section.

Following Refs. [13,27] we assume that the dominant contribution to the loop integrals comes from their pole terms. The consideration of the regular parts with off-shell kaons needs incorporation of the corresponding off-shell form factors, which brings an additional ambiguity into the model. Thus, our estimate may be considered as a lower bound of the coherence effect. The pole part may be evaluated by summing all possible cuttings of the loops, as shown in Fig. 9. Calculating the imaginary parts we use the following substitutions for the propagators of the on-shell particles (Cutkovsky rules [28]), shown by crosses in Fig. 9,

$$\begin{aligned}\frac{1}{q^2-M_K^2} &\to -2\pi i\,\delta\big(q^2-M_K^2\big),\\ \frac{\not p + M}{p^2-M^2} &\to -2\pi i\,(\not p + M)\,\delta(p^2-M^2)\end{aligned} \tag{6}$$

and the identity

$$\int d^4p\,\delta(p^2-M^2) = \int\frac{d^3\mathbf{p}}{2E_p} \tag{7}$$

with $E_p^2 = \mathbf{p}^2 + M^2$. We also use the standard representation of the product of the deuteron vertex function and the attached nucleon propagator through the nonrelativistic deuteron wave

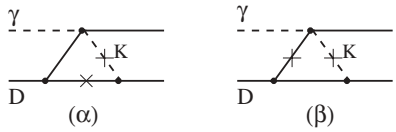

FIG. 9. Diagrammatic representation of cutting (indicated by crosses) the loop diagrams.

function

$$\Gamma_D\frac{\bar u_{m_1}\bar u_{m_2}}{p'^2-M_N^2}U_{m_D} = \sqrt{2M_D}\,\phi^{m_D}_{m_1m_2}, \tag{8}$$

where $p' = p_D - p$ and $\phi^{m_D}_{m_1m_2}$ is the deuteron wave function with the spin projection m_D and the nucleon spin projections m_1 and m_2. By using Eqs. (6)–(8), one can express the principal parts of the invariant amplitudes in Eq. (5) as

$$\begin{aligned}A^P &= \sum_{\xi=\alpha,\beta}A^P(\xi),\\ A^P(\xi) &= i\frac{\sqrt{2M_D}}{16\pi}\sum_{m_1m_2}\int\frac{p\,dp}{E_p|\mathbf{p}_\xi|}T^{\Lambda^*}_{m_1}(\xi)\Gamma^{*\Theta^+}_{m_2}(\xi)\\ &\quad\times\theta[1-a(p,\mathbf{p}_\xi)]\,\phi^{m_D}_{m_1m_2}[p,a(p,\mathbf{p}_\xi)],\end{aligned} \tag{9}$$

where $\mathbf{p}_\xi$ is the spatial component of the corresponding four-vectors, defined as $p_\alpha = p_{\Theta^+}$ and $p_\beta = p_Y - k_\gamma$. Indices α and β refer to the left and right cutting diagrams in Fig. 9, respectively. The function $a(p,\mathbf{p}_\xi)$ is the cosine of the polar angle of the internal nucleon momentum $\mathbf{p}$ in a deuteron when the z axis is along the momentum $\mathbf{p}_\xi$.

$$a(p,\mathbf{p}_\xi) \equiv \cos\theta_p = \frac{M_K^2 - M_\xi^2 - M_N^2 + 2E_\xi E_p}{2|\mathbf{p}||\mathbf{p}_\xi|}, \tag{10}$$

with $\xi = \alpha, \beta$ and $M^2_{\alpha,\beta} = p^2_{\alpha,\beta}$.

The Λ^* photoproduction and Θ^+ decay amplitudes read

$$\begin{aligned}T^{\Lambda^*}_{m_1}(\alpha) &= \bar u^\sigma_{\Lambda^*}(p^*_\Lambda)\mathcal{M}^{\Lambda^*}_{\sigma\mu}\,\epsilon^\mu u_{m_1}(p')\,\theta(m'^2),\\ T^{\Lambda^*}_{m_1}(\beta) &= \bar u^\sigma_{\Lambda^*}(p^*_\Lambda)\mathcal{M}^{\Lambda^*}_{\sigma\mu}\,\epsilon^\mu u_{m_1}(p),\\ \Gamma^{\Theta^+}_{m_2}(\alpha) &= \bar u_{m_2}(p)\gamma_5 u_\Theta(p_\Theta),\\ \Gamma^{\Theta^+}_{m_2}(\beta) &= \bar u_{m_2}(p')\gamma_5 u_\Theta(p_\Theta)\,\theta(m'^2),\\ p' &= p_D - p,\\ m'^2 &= p'^2_0 - \mathbf{p}'^2.\end{aligned} \tag{11}$$

Now we have an additional cut $m'^2 > 0$, compared to Ref. [13], that suppresses the integrals in Eq. (9) and reduces the values of the corresponding cross sections. The effective deuteron vertex reads

$$\phi^{m_D}_{m_1m_2}(p,a) = 4\pi\sum_{Lm_Lm_s}\left\langle\frac{1}{2}m_1\frac{1}{2}m_2\middle|1m_s\right\rangle \times\langle 1m_sLm_L|1m_D\rangle\,i^L u_L(p)Y_{Lm_L}(\widehat{\mathbf{p}}), \tag{12}$$

where a is the cosine of the polar angle of $\mathbf{p}$, $u_L(p)$ denotes the deuteron wave function in momentum space

$$u_L(p) = \int u_L(r)\,j_L(pr)\,r\,dr, \tag{13}$$

normalized as

$$\frac{2}{\pi}\int p^2\left[u_0^2(p)+u_2^2(p)\right]dp = 1. \tag{14}$$

In our calculation we use the deuteron wave function derived from the "realistic" Paris potential. We checked that the final result does not depend on the fine details of the deuteron wave function and practically does not depend on the choice of the potential.

Calculating the loop integrals in Eq. (9), one has to be careful with the proper determination of the three-momentum of **p** which is the argument of the corresponding elementary amplitudes in the integrals. The azimuthal angle of **p** is chosen to be zero because all momenta are in the production plane. To get the internal momentum **p** in the laboratory system with the z axis along the beam direction, we make the following transformation

$$\begin{aligned} p_x &\to p_x\cos\theta_\xi - p_z\sin\theta_\xi \\ p_z &\to p_x\sin\theta_\xi + p_z\cos\theta_\xi, \end{aligned} \tag{15}$$

where θ_ξ is the polar angle of momentum p_ξ.

The differential cross section of the associated pK^- and NK photoproduction, integrated over the pK^- invariant mass in the range $M_Y = M_{\Lambda^*} \pm 20$ MeV at $M_X = M_{\Theta^+}$, is related to the differential cross section of the associated $\Lambda^*\Theta^+$ photoproduction as

$$\left.\frac{d\sigma^{\gamma D\to pK^-X}}{d\cos\theta\, dM_X}\right|_{M_X=M_{\Theta^+}} \simeq \frac{N}{\pi\Gamma_{\Theta^+}}\frac{d\sigma^{\gamma D\to\Lambda^*\Theta^+}}{d\cos\theta}, \tag{16}$$

where $N \simeq 0.17$ is the integral over the Breit-Wigner $\Lambda^* \to pK^-$ decay distribution

$$N = B_{pK^-}\int_{M_{\Lambda^*}-\Delta}^{M_{\Lambda^*}+\Delta}\frac{2M_{\Lambda^*}M_X\Gamma_{\Lambda^*}dM_X}{\left(M_X^2-M_{\Lambda^*}^2\right)^2+(M_{\Lambda^*}\Gamma_{\Lambda^*})^2} \tag{17}$$

with $\Delta = 20$ MeV and the branching ratio $B_{pK^-} \simeq 0.45/2$.

The differential cross section of the coherent $\Lambda^*\Theta^+$ photoproduction reads

$$\frac{d\sigma^{\gamma D\to\Lambda^*\Theta^+}}{d\cos\theta} = \frac{1}{32\pi}\frac{1}{s_D}\frac{p_f}{p_i}|A_a + A_b|^2, \tag{18}$$

where A_a and A_b are the amplitudes of the charge and neutral current exchange, respectively, depicted in Fig. 1. In this equation, averaging and summing over the spin projections in the initial and the final states are performed. The difference between A_a and A_b consists of different elementary amplitudes for the $\gamma p \to \Lambda^* K^+$ and $\gamma n \to \Lambda^* K^0$ reactions, and in an opposite sign of the $\Theta^+ nK^+$ and $\Theta^+ pK^0$ couplings which is a consequence of the zero isospin of Θ^+. The relative sign of the amplitudes of $\gamma p \to \Lambda^* K^+$ and $\gamma n \to \Lambda^* K^0$ follows the relative sign of the $\gamma \bar{K}^{0^*} K^0$ and $\gamma K^{-*} K^+$ coupling constants and, according to SU(3) predictions, is opposite. Therefore, the sum of the charged and neutral K meson exchange diagrams leads to a constructive interference between A_a and A_b, and an enhancement of the cross section of the associated $\Lambda^*\Theta^+$ photoproduction.

In Fig. 10 we show the average momenta $\langle\langle p_\alpha\rangle\rangle$ and $\langle\langle p_\beta\rangle\rangle$ in the loop diagrams depicted in Figs. 9 [(α) and (β), respectively] as a function of the pK^- photoproduction angle in the c.m. system. This example corresponds to $E_\gamma = 2.1$ GeV and $M_0 = 1.52$ GeV. The definition of this averaging is given as usual,

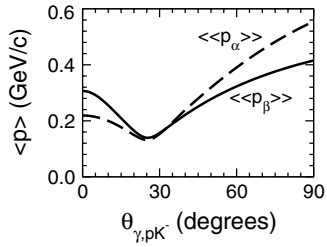

FIG. 10. The average momenta $\langle\langle p_\alpha\rangle\rangle$ and $\langle\langle p_\beta\rangle\rangle$ in the loop diagrams shown in Figs. 9 [(α) and (β), respectively] as a function of the pK^- photoproduction angle.

$$\langle\langle p\rangle\rangle^2 = \frac{\int dM_X d\Omega_X d\Omega_Y \langle p\rangle^2}{\int dM_X d\Omega_X d\Omega_Y}, \tag{19}$$

with

$$\langle p\rangle = \frac{\int pF(p)dp}{\int F(p)dp}, \tag{20}$$

where $F(p)$ is the integrand in the loop integrals. One can see that the average momenta have a minimum at $\theta \sim 25^\circ$. Near this position the corresponding amplitudes have a maximum. At large angles, mean values of p are large and, as a result, the corresponding amplitudes are very small because of the exponentially small value of the deuteron wave function at large p.

In Fig. 11 we show the angular distribution of the differential cross section $d\sigma/d\Omega dM_X$ of the $\gamma D \to \Theta^+ pK^- \to pK^- X$ reaction at $E_\gamma = 2.1$ GeV, and the missing mass $[\gamma D, pK^-]$, $M_X = M_{\Theta^+} = 1.53$ GeV, and at $M_0 = M_{\Lambda^*} = 1.52$ and 1.62 GeV in (a) and (b), respectively. The solid curves correspond to the resonance contribution, i.e., $\gamma D \to \Lambda^*\Theta^+ \to pK^- X$, whereas the dashed curves shows the contribution from the nonresonant $\gamma N \to pK^- K$ processes depicted schematically in Fig. 12.

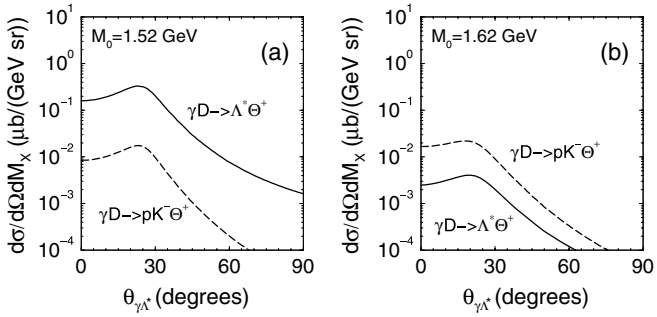

FIG. 11. The angular distribution of the differential cross section $d\sigma/d\Omega dM_X$ at $M_X = M_{\Theta^+} = 1.53$ GeV, $E_\gamma = 2.1$ GeV, and $M_0 = M_{\Lambda^*} = 1.52$ and 1.62 (GeV), shown in (a) and (b), respectively. The solid and dashed curves correspond to resonant and coherent background contributions.

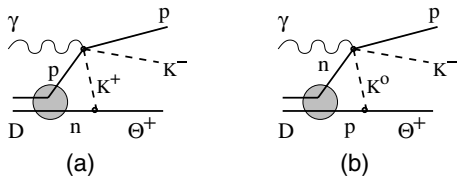

FIG. 12. Diagrammatic representation of the associated nonresonant $pK^-\Theta^+$ photoproduction.

One can see that in the Λ^* region, where $M_0 = M_{\Lambda^*}$, the resonant cross section is about one order of magnitude larger than the contribution of the nonresonant channels discussed in the previous section. Outside the resonance position, say for $M_0 = M_{\Lambda^*} + 100$ MeV, the result is opposite, namely the resonant contribution is strongly suppressed because of a small Λ^* total decay width, and the processes with nonresonant $\gamma N \to pK^-K$ transitions become dominant. In Figs. 13(a) and 13(b) we show the resonant cross section as a function of the Λ^* photoproduction angle in the c.m. system and the laboratory system, respectively, for several values of the photon energy. The value of the cross section at maximum and the position of the maximum depends on the energy. One can see that the Θ^+ formation in associated $\Lambda^*\Theta^+$ photoproduction is hardly measurable if the detector acceptance does not allow measuring the pK^- pairs at small angles $\theta_{\rm lab} \leqslant 10^\circ$.

Finally, let us discuss the dependence of the associated $\Lambda^*\Theta^+$ photoproduction on the spin and parity of the Θ^+. The case of $J^P_\Theta = 3/2^-$ is especially attractive because the small Θ^+ decay width [26] has a natural explanation for this assignment of the Θ^+ spin and parity [29–32].

The effective Lagrangians of the Θ^+NK interactions are expressed usually in the following form [31]

$$\mathcal{L}^{\frac{1}{2}^\pm}_{\Theta NK} = g^{\frac{1}{2}^\pm}_{\Theta NK}\bar\Theta\Gamma^\pm K N + \text{h.c.}, \tag{21}$$

$$\mathcal{L}^{\frac{3}{2}^\pm}_{\Theta NK} = \frac{g^{\frac{3}{2}^\pm}_{\Theta NK}}{M_\Theta}\bar\Theta^\alpha\Gamma^\mp(\partial_\alpha K)N + \text{h.c.}, \tag{22}$$

where Θ, N, and K are the Θ^+, nucleon, and kaon fields; $\Gamma^+ = \gamma_5$; and $\Gamma^- = 1$. For the fixed $\Theta^+ \to NK$ decay width the coupling constant $g_{\Theta NK}$ depends on the spin and parity of Θ^+ as

$$\left|g^{\frac{1}{2}^\pm}_{\Theta NK}\right|^2 = \frac{4\pi\Gamma_\Theta}{p_F}\frac{M^2_\Theta}{(M_\Theta \mp M_N)^2 - M^2_K},$$
$$\left|g^{\frac{3}{2}^\pm}_{\Theta NK}\right|^2 = \frac{48\pi\Gamma_\Theta}{p_F}\frac{M^6_\Theta}{\lambda\big(M^2_\Theta, M^2_N, M^2_K\big)\big[(M_\Theta \pm M_N)^2 - M^2_K\big]}, \tag{23}$$

where $p_F = \sqrt{\lambda(M^2_\Theta, M^2_N, M^2_K)}/2M_\Theta$ is the Θ^+ decay momentum. These equations result in the following relation

$$\left|g^{\frac{1}{2}^-}_{\Theta NK}\right| : \left|g^{\frac{1}{2}^+}_{\Theta NK}\right| : \left|g^{\frac{3}{2}^+}_{\Theta NK}\right| : \left|g^{\frac{3}{2}^-}_{\Theta NK}\right| = 0.134 : 1 : 1.39 : 10.21, \tag{24}$$

where, for example for $\Gamma_\Theta = 1$ MeV, $|g^{\frac{1}{2}^+}_{\Theta NK}| = 1.04$. Using this estimate one can expect naively that in case of $J^P = \frac{3}{2}^-(\frac{1}{2}^-)$ the coherent $\Lambda^*\Theta^+$ photoproduction would be enhanced (suppressed) roughly by two orders of magnitude compared to the case of $J^P = 1/2^+$. But the real situation is far from this expectation. The matrix elements defining the Θ^+ formation are proportional to the products

$$g_{\Theta^+NK} \times t_{m_\Theta m_N} \tag{25}$$

with

$$t^{\frac{1}{2}^\pm}_{m_\Theta m_N} = \bar u_{\Theta m_\Theta}\Gamma^\pm u_{m_N},$$
$$t^{\frac{3}{2}^\pm}_{m_\Theta m_N} = \bar u^\alpha_{\Theta m_\Theta}\Gamma^\mp q_\alpha u_{m_N}, \tag{26}$$

where q is the kaon momentum and m_Θ and m_N denote the spin projections of Θ^+ and nucleon, respectively. As a result, the large (small) value of $|g_{\Theta NK}|$ is compensated by the corresponding small (large) value of t_{m_Θ, m_N}. For a qualitative estimate of such a compensation let us consider the combination

$$|A|^2 = \sum_{m_\Theta m_N} |g_{\Theta NK}\, t_{m_\Theta, m_N}|^2, \tag{27}$$

where the nucleon may be off-shell and express $|A|^2$ through the Θ^+ decay width

$$\left|A^{\frac{1}{2}^\pm}\right|^2 = 8\pi M^2_\Theta\frac{\Gamma_\Theta}{p_F}\frac{(M_\Theta \mp \bar M_N)^2 - M^2_K}{(M_\Theta \mp M_N)^2 - M^2_K},$$
$$\left|A^{\frac{3}{2}^\pm}\right|^2 = 16\pi M^2_\Theta\frac{\Gamma_\Theta}{p_F}\frac{\lambda\big(M^2_\Theta, \bar M^2_N, M^2_K\big)}{\lambda\big(M^2_\Theta, M^2_N, M^2_K\big)}\frac{(M_\Theta \pm \bar M_N)^2 - M^2_K}{(M_\Theta \pm M_N)^2 - M^2_K}, \tag{28}$$

where $\bar M^2_N = p^2 > 0$ is the square of the nucleon momentum in the Θ^+NK vertex. From these equations one can conclude that in case of an on-shell nucleon with $\bar M^2_N = M^2_N$: (i) $|A|^2$ does not depend on parity and (ii) $|A^{\frac{3}{2}}|^2 = 2|A^{\frac{1}{2}}|^2$. The latter is the consequence of the spin factor $2J + 1$ in the expression for the decay width. The dependence on parity arises only for off-shell nucleons. $|A|^2$ increases (decreases) for $J^P = 1/2^+$ and $3/2^\pm(1/2^-)$ at the off-shell region with $\bar M^2_N < M^2_N$. The increase for $J^P = 3/2^+$ and $3/2^-$ is different, because in the former case $|A|^2$ is defined by the interplay of suppression and

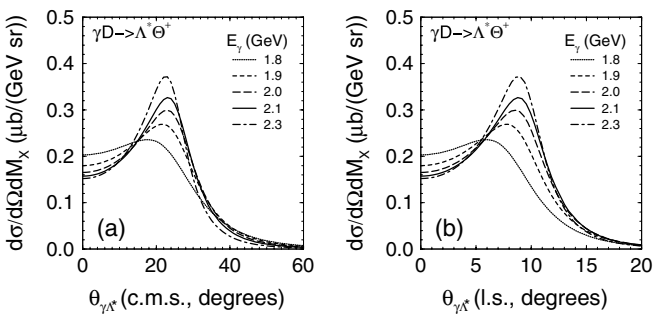

FIG. 13. The same as in Fig. 11 but for different E_γ. (a) and (b) correspond to the dependence on the Λ^* photoproduction angle in the c.m. system and the laboratory frame, respectively.

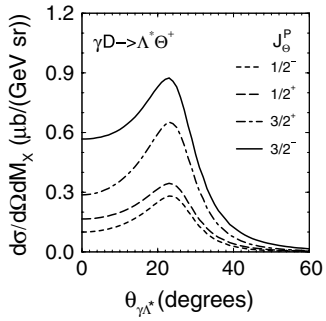

FIG. 14. The same as in Fig. 13(a), but for different Θ^+ spin and parities. $E_\gamma = 2.1$ GeV and $M_0 = 1.52$ GeV.

enhancement factors. On average, the ratio of $|A^{\frac{3}{2}}|^2/|A^{\frac{1}{2}}|^2$ would be slightly larger than 2.

In some sense, the dependence of the amplitude of the associated $\Lambda^*\Theta^+$ photoproduction on spin and parity of the Θ^+ is rather similar to that of A^{J^P} in our example. The diagrams with the on-shell hadrons in the Θ^+ formation vertex [see (α) in Fig. 9] do not depend on Θ^+ parity, and for $J = 3/2$ their contribution is roughly two times greater than for $J = 1/2$. The amplitudes with the off-shell nucleon in the Θ^+ formation vertex [(β) in Fig. 9] are enhanced for $J^P = 1/2^+, 3/2^\pm$ and suppressed for $J^P = 1/2^-$. But this off-shell modification is not so large, because the contribution of the nucleons that are far off-shell are suppressed by the deuteron wave function.

In Fig. 14 we show the angular distribution of the differential cross section $d\sigma/d\Omega dM_X$ at $M_X = M_{\Theta^+} = 1.53$ GeV, and $E_\gamma = 2.1$ GeV, $M_0 = M_{\Lambda^*} = 1.52$ and different Θ^+ spin and parities, $J^P = \frac{1}{2}^\mp$ and $\frac{3}{2}^\pm$. The ratio of the cross section at their maximum position for different J^P reads

$$\frac{1}{2}^- : \frac{1}{2}^+ : \frac{3}{2}^+ : \frac{3}{2}^- \simeq 0.81 : 1 : 1.87 : 2.53. \qquad (29)$$

This result is in agreement with our qualitative analysis, namely the cross section for $J = 3/2$ on average is 2.4 times greater than for $J = 1/2$. For $J^P = 1/2^+$ and $3/2^-$ the cross sections are enhanced compared to the cases of $J^P = 1/2^-$ and $3/2^+$, respectively.

Now two questions arise. First, whether the associated $\Lambda^*\Theta^+$ photoproduction may be seen against other nonresonant processes in the resonance region with $M_0 = M_{\Lambda^*}$ and, second, whether this signal is suppressed outside the resonance region and why? To answer these questions we have to analyze the background processes.

V. NONRESONANT BACKGROUND

A. Spectator channels

The spectator channels are depicted in Fig. 15. Contributions of these channels to the invariant mass distribution are defined by Eqs. (1) and (2), where the amplitudes are expressed via products of the amplitude of the elementary $\gamma N \to N\bar{K}K$

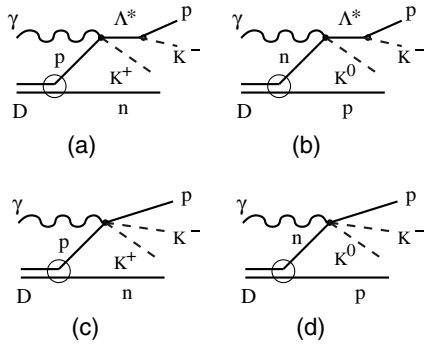

FIG. 15. Diagrammatic representation of background spectator channels. [(a) and (b)] Quasifree Λ^*K photoproduction; [(c) and (d)] quasifree nonresonant pK^-K photoproduction.

reactions $A^{\gamma N}(n)$ and the deuteron wave function ϕ as

$$T_{fi}(n) = \sqrt{2M_D} \sum_m A^{\gamma N}_{m_2;m\lambda}(n)\phi^{m_D}_{m,m_1}(\mathbf{p}), \qquad (30)$$

where the deuteron wave function is defined in Eq. (12) and the index n corresponds to the different elementary subprocesses discussed in Sec. III. The background contributions for the quasifree Λ^* photoproduction, vector-meson, and hyperon excitations are shown in Fig. 16 by solid, dot-dashed, and long-dashed curves, respectively. If the pK^- invariant mass is close to the Λ^* mass [cf. Fig. 16(a)] the quasifree Λ^* photoproduction gives the dominant contribution to the background. The next important contribution comes from the BG_Y channel, parameterized by the constant matrix element. The contribution of the vector mesons in the region where the $[\gamma D, pK^-]$ missing mass is around the Θ^+ mass is rather small. Indeed, it does not contribute to the γn reaction and, moreover, it is suppressed dynamically. Thus, the kinematics of the associated $\Lambda^*\Theta^+$ photoproduction in the forward direction requires a fast K^- and slow K^+. In this case, the K^+K^- invariant mass is far from the ϕ meson mass. But the situation changes at large values of the $[\gamma D, pK^-]$ missing mass. In this case the available values of K^+K^- invariant mass cover the ϕ meson mass region, and the contribution of the ϕ meson excitation becomes essential. The case when the pK^- invariant

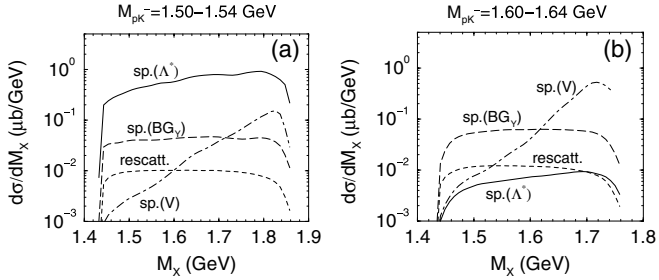

FIG. 16. Background contributions to the missing-mass distribution in the $\gamma D \to pK^- X$ reaction at $E_\gamma = 2.1$ GeV for quasifree Λ^* photoproduction, vector-meson, and hyperon excitations (spectator mechanism), and rescattering channels shown by solid, dot-dashed, long-dashed, and dashed curves, respectively. (a) and (b) correspond to $M_0 = 1.52$ and 1.62 GeV, respectively.

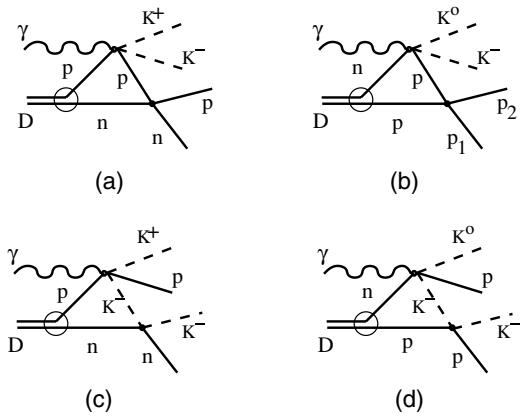

FIG. 17. Rescattering of the proton (a and b) and K^- meson (c and d) in the pK^-NK photoproduction from the deuteron.

mass is far from the Λ^* mass is shown in Fig. 16(b). Now, the quasifree Λ^* photoproduction is suppressed, whereas the other channels have the same order of magnitude.

B. Rescattering processes

Let us consider proton and K^- meson rescattering when a pK^- pair is produced in the γN interaction as shown in Figs. 17(a)–17(d), respectively. In principle, the K^+n and K^0p rescattering in quasifree $\gamma N \to pK^-K$ photoproduction from a deuteron must be taken into account, too, but we skip them at the present stage, assuming first that such processes give a small correction to the spectator (quasifree photoproduction) channels considered in the previous section and, second, the cross section for elastic K^+N scattering is much smaller than for K^-N scattering [25]. Moreover, as we show, the dominant contribution here comes from proton rescattering and, therefore, kaon rescattering is a small part. Basically, the amplitudes of the rescattering processes are evaluated similarly to the amplitudes of the associated coherent $\Theta^+\Lambda^*$ or Θ^+pK^- photoproduction considered in Sec. III, where we assumed the dominance of the imaginary part of the corresponding loop diagrams, calculated by cutting rules. But there are several new aspects.

First, the rescattered particles are outside of the production plane and, therefore, now, in the loop integrals we have to integrate over the virtual nucleon momentum p and the azimuthal angle φ_p. If the polar and azimuthal angles of the momentum $\mathbf{p}_\xi$ are θ_ξ and φ_ξ, respectively, then the three-dimensional vector of the virtual nucleon in the laboratory frame, with the z axis along the beam direction, reads

$$\begin{aligned} p_x &= p'_x \cos\varphi_\xi - p'_y \sin\varphi_\xi, \\ p_y &= p'_y \cos\varphi_\xi + p'_x \sin\varphi_\xi, \\ p_z &= p(\cos\theta_p \cos\theta_\xi - \sin\theta_p \sin\theta_\xi \cos\varphi_p), \end{aligned} \tag{31}$$

where

$$\begin{aligned} p'_x &= p(\sin\theta_p \cos\varphi_p \cos\theta_\xi + \cos\theta_p \sin\theta_\xi), \\ p'_y &= p \sin\theta_p \sin_p \varphi_p. \end{aligned}$$

The polar angle θ_p is fixed by the on-shell conditions [cf. Eq. (10)]

$$a(p, \mathbf{p}_\xi) \equiv \cos\theta_p = \frac{M_K^2 - M_\xi^2 - M_N^2 + 2E_\xi E_p}{2|\mathbf{p}||\mathbf{p}_\xi|}, \tag{32}$$

where the four-momenta $p_\xi = p_{(\alpha,\beta)}$ are defined as follows:

p rescattering:

$$p_\alpha = p_N + p_f, \quad p_\beta = p_K + p_{K^-} - k_\gamma, \tag{33}$$

K^- rescattering:

$$p_\alpha = p_N + p_{K^-}, \quad p_\beta = p_f + p_K - k_\gamma, \tag{34}$$

where p_N and p_f refer to the momenta of the outgoing nucleon and the proton of the X and Y systems, respectively. We remind the reader that the indices α and β refer to the cut loops shown in (α) and (β), respectively, in Fig. 9. To preserve the energy-momentum conservation in the loop vertices one has to be careful with the determination of the azimuthal angles φ_ξ. The corresponding expression reads

$$\begin{aligned} \varphi_\xi &= \bar\varphi_\xi \theta(s_\xi) + (2\pi - \bar\varphi_\xi)\theta(-s_\xi), \\ \cos\bar\varphi_\xi &= \frac{p_{\xi_x}}{|\mathbf{p}_\xi| \sin\theta_\xi}, \\ s_\xi &= \frac{p_{\xi_y}}{|\mathbf{p}_\xi| \sin\theta_\xi}. \end{aligned} \tag{35}$$

Next, one has to choose the effective amplitudes in the loop integrals. We take them as a product of the deuteron wave function, photoproduction of the K^-K pair in $\gamma N \to pK^-K$ reaction, and elastic-scattering amplitudes. For the proton and K^-meson rescattering they read correspondingly

$$\begin{aligned} T^p_{m_p m_N; m_D \lambda} &= \sqrt{2M_D} \sum_{m m_1 m_2} T^{\gamma N \to pKK^-}_{m, m_1 \lambda} \\ &\quad \times T^{pN \to pN}_{m_p m_N, m m_2} \phi^{m_D}_{m_1 m_2}[p, a(p, \mathbf{p}_\xi)], \\ T^{K^-}_{m_p m_N; m_D \lambda} &= \sqrt{2M_D} \sum_{m_1 m_2} T^{\gamma N \to pKK^-}_{m_p, m_1 \lambda} \\ &\quad \times T^{K^-N \to K^-N}_{m_N, m_2} \phi^{m_D}_{m_1 m_2}[p, a(p, \mathbf{p}_\xi)], \end{aligned} \tag{36}$$

where m_p and m_N are the spin projections of the outgoing proton and nucleon, respectively. In our calculations we use an on-shell approximation for the elastic-scattering amplitudes $T^{pN \to pN}_{fi}$ and $T^{K^-N \to K^-N}_{fi}$, taken from the experimentally measured cross sections of elastic scattering. Details of the employed parameterizations are given in Appendix B.

An important point is related to the $\gamma N \to pKK^-$ vertex. In our model it consists of three components: Λ^* excitation, the vector-meson contribution, and the remaining background contribution denoted above as BG_Y. Consider first the Λ^* channel. Due to the rescattering kinematics, the invariant mass of the virtual pK^- pair in the loop integrals covers the Λ^* resonance region even when the invariant mass of the outgoing p and K^- meson is outside the resonance position. This results in increasing the background contribution at $M_0 \neq M_{\Lambda^*}$. But the situation is not so simple. Because the Λ^* has a small total decay width, $\Gamma_{\rm tot} \simeq 15.6$ MeV, its decay length is large,

$$l_0 = v t_0 = \frac{v}{c} \frac{\hbar c}{\Gamma_{\rm tot}} \simeq 6\text{–}10 \text{ fm}, \tag{37}$$

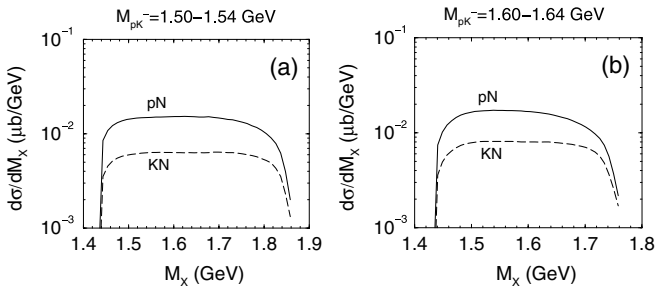

FIG. 18. The pN and K^-N rescattering channels in $\gamma D \to pK^- X$ reaction at $E_\gamma = 2.1$ GeV for $M_0 = 1.52$ and 1.62 GeV shown in (a) and (b), respectively.

at a Λ^* velocity $v \sim (0.5\text{–}0.8)\,c$. In other words, the Λ^* decays mostly outside of the deuteron. Similar or even larger suppression is expected for the case of the ϕ-meson contribution. Therefore, we can simply neglect these two channels.

In Fig. 18 we show the relative contributions of p and K^- rescattering for different channels. Enhancement of the p rescattering is explained by the difference between the cross sections for pN and K^-N elastic scattering.

To summarize this section we conclude that at low energy, say $E_\gamma = 1.7\text{–}2.3$ GeV, the dominant component of the nonresonant background comes from the quasifree Λ^* spectator channel, the next important contribution is composed of the BG_Y spectator channel and pN rescattering, if the invariant mass of the pK^- pair is inside the Λ^* resonance position with $M_0 = 1.52$ GeV. Outside of the Λ^* resonance position the quasifree Λ^* spectator channel is strongly suppressed, whereas other channels remain on the same level.

Finally, let us examine the angular dependence of the spectator channel, similar to the associated $\Lambda^*\Theta^+$ photoproduction (cf. Figs. 13 and 14). The corresponding result is shown in Fig. 19 where we present simultaneously contributions from the associated $\Lambda^*\Theta^+$ photoproduction (signal) and from the background (noise) dominated by the spectator channels. The calculation is for the resonance region with $M_X = 1.53$ GeV, $M_0 = 1.52$ GeV, and $E_\gamma = 2.1$ GeV. We choose the case of $J^P_\Theta = 3/2^-$. One can see that the spectator channel has a sharp peak caused by the deuteron wave function with a maximum

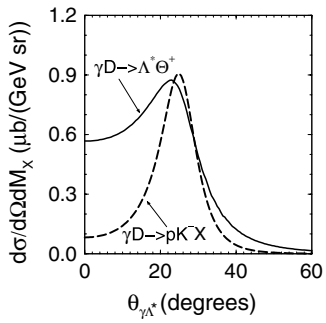

FIG. 19. The angular dependence of the missing mass distribution for the associated $\Lambda^*\Theta^+$ (solid curve) photoproduction and the background spectator processes (dashed curve) at $M_X = 1.53$ GeV, $M_0 = 1.52$ GeV, and $E_\gamma = 2.1$ GeV.

close to the maximum for coherent $\Lambda^*\Theta^+$ photoproduction. At small angles the noise decreases much faster than the signal. Therefore, we can conclude that the largest value for the S/N ratio is expected at extremely forward pK^- photoproduction angles, say $\theta_{\text{c.m.s.}} \leqslant 22^\circ$.

VI. RESULTS AND DISCUSSION

Below, we discuss the prediction for the Θ^+ formation processes under two different conditions. The first is Θ^+ photoproduction at low energy ($E_\gamma = 1.7\text{–}2.3$ GeV) in the inclusive $\gamma D \to pK^- X$ reaction. It can be studied, for example, by LEPS at SPring-8 and/or Crystal-Barrel at ELSA (Bonn). The second is the formation Θ^+ photoproduction process in exclusive $\gamma D \to pK^- nK^+$ reaction in a wider energy interval ($E_\gamma = 1.7\text{–}3.5$ GeV) with the experimental conditions of the CLAS Collaboration measurement [7]. All calculations are made for a total Θ^+ decay width of $\Gamma_\Theta = 1$ MeV.

A. The missing mass distribution in inclusive $\gamma D \to pK^- X$ reactions

We calculate the missing mass distribution in the inclusive $\gamma D \to pK^- X$ reaction with two cuts. The first one is the ϕ-meson cut. We exclude all events with a K^+K^- invariant mass close to the mass of the ϕ meson: $|M_{K^+K^-} - M_\phi| < 20$ MeV [1]. The second one is the angular cut: we keep only forward pK^- pair photoproduction with $\theta_{\text{c.m.s.}} \leqslant 22^\circ$. This cut gives a maximum S/N ratio. Hereafter, we define the corresponding missing mass distribution as $d\sigma^F/dM_X$, where the superscript F indicates, conditionally, an alignment in the forward photoproduction of the pK^- pair. Figure 20 illustrates the effect of the angular cut in the missing mass distribution $\gamma D \to pK^- X$ reaction at the Λ^* resonance position with $M_{pK^-} \sim M_{\Lambda^*}$ ($M_0 = 1.52$ GeV), averaging over the energy interval $E_\gamma = 1.7\text{–}2.3$ GeV. Here, we choose the case of $J^P_\Theta = 3/2^-$. First, in the Λ^* resonance region one can see a distinct effect of the associated $\Lambda^*\Theta^+$ photoproduction as a sharp Θ^+ peak against the flat nonresonant background with

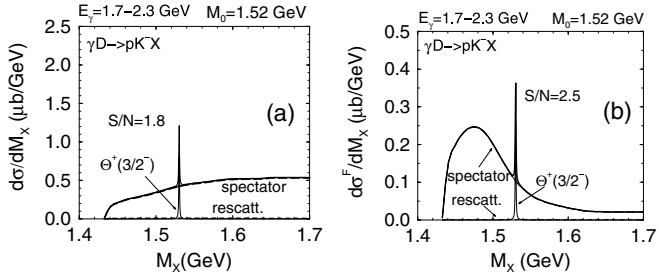

FIG. 20. The $[\gamma D,\, pK^-]$ missing mass distribution in the $\gamma D \to pK^- X$ reaction together with the partial contributions of different background channels at $M_0 = 1.52$ GeV and $E_\gamma = 1.7\text{–}2.3$ GeV. The contributions from the Θ^+ signal, spectator and rescattering processes are shown by the thin, long dashed, and dashed curves, respectively. (a) and (b) correspond to calculations without and with the angular cut $\theta_{pK^-} \leqslant 22^\circ$, respectively.

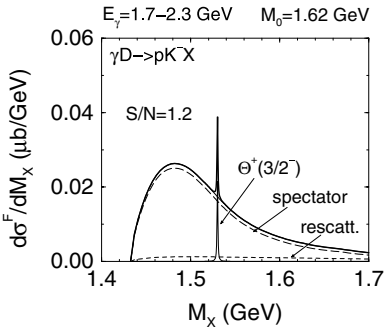

FIG. 21. The same as in Fig. 20(b) but for $M_0 = 1.62$ GeV.

and without the angular cut. The angular cut increases the S/N ratio. Figure 20(a) shows the missing mass distribution calculated for $\theta_{pK^-} \leqslant \pi/2$ (c.m. system), whereas in Fig. 20(b) the angular interval is limited to 22° in accordance with the results in Fig. 19. The angular cut suppresses the cross sections of both the Θ^+ signal and the background; it further modifies the shape of the background in such a way as to get the maximum S/N ratio at the resonance position $M_X = M_\Theta$. The shape modification is explained by the suppression of the quasifree spectator channel at large invariant mass M_X. When M_X increases the maximum in the quasifree background distribution, shown in Fig. 19 (dashed curve), moves toward large angles being outside of the integration region and, therefore, the contribution of this channel decreases. As a result, the angular cut creates an enhancement of the S/N ratio by about 40%.

Figure 21 illustrates the case when the pK^- invariant mass is far from the Λ^* resonance position, $M_0 = 1.62$ GeV. Now we also see some Θ^+ peak generated mainly by the associated nonresonant processes. The resonance channel is suppressed because of the small Λ^* decay width. The background near the Θ^+ peak is dominated by the BG_Y and rescattering channels. Because now the charged and neutral K-meson exchange diagrams contribute incoherently, the ratio $(S/N)_{\rm NR}$ would be smaller compared to the ratio in the resonance region, $(S/N)_R$. Neglecting the rescattering channels and the background shape modification, one can get the following qualitative estimate

$$\left(\frac{S}{N}\right)_{\rm NR} \simeq \frac{1}{2}\left(\frac{S}{N}\right)_R. \tag{38}$$

The background shape modification and the rescattering channels result in decreasing $(S/N)_{\rm NR}$.

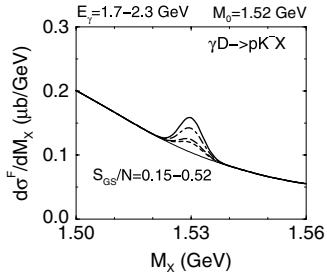

FIG. 23. The missing mass distribution for $\gamma D \to pK^-NK$ at $E_\gamma = 1.7$–2.3 GeV and $M_0 = 1.52$ GeV and for different Θ^+ spin and parity, folded with a Gaussian resolution function.

In Fig. 22 we show the missing mass distribution for different Θ^+ spin and parity: $J^P = \frac{1}{2}^\mp, \frac{3}{2}^\pm$. The signal-to-noise ratio for different J^P reads

$$\tfrac{1}{2}^- : \tfrac{1}{2}^+ : \tfrac{3}{2}^+ : \tfrac{3}{2}^- \simeq 0.7 : 0.9 : 1.7 : 2.5. \tag{39}$$

This result is in qualitative agreement with the previous analysis of the differential invariant mass distributions [cf. Eq. (29)].

Note that the value of the invariant mass distribution at the resonance is independent of the Θ^+ decay width. But because all experiments have a finite experimental resolution, the measured signal is smeared by the experimental resolution, and this smeared signal must depend on the value of Γ_Θ. In Fig. 23 we show the missing mass distribution folded with a Gaussian distribution function

$$\frac{d\sigma}{dM_X} = \int \frac{d\sigma}{dM} f(M_X - M)dM,$$
$$f(M_X - M) = \frac{1}{\sigma\sqrt{2\pi}} \exp\left[-\frac{(M_X - M)^2}{2\sigma^2}\right], \tag{40}$$

with $\sigma = 3$ MeV, which imitates a finite experimental resolution. The symbol $S_{\rm GS}/N$ means the signal-to-noise ratio in missing mass distribution folded with a Gaussian resolution function. In this case, the height of the resonance peak (S) decreases proportional to the factor of

$$\frac{\sqrt{\pi}}{2\sqrt{2}}\frac{\Gamma_\Theta}{\sigma} \simeq 0.21. \tag{41}$$

Therefore, to see this peak above the background, one needs rather good experimental resolution, even assuming that the Θ^+ spin-parity is $3/2^-$.

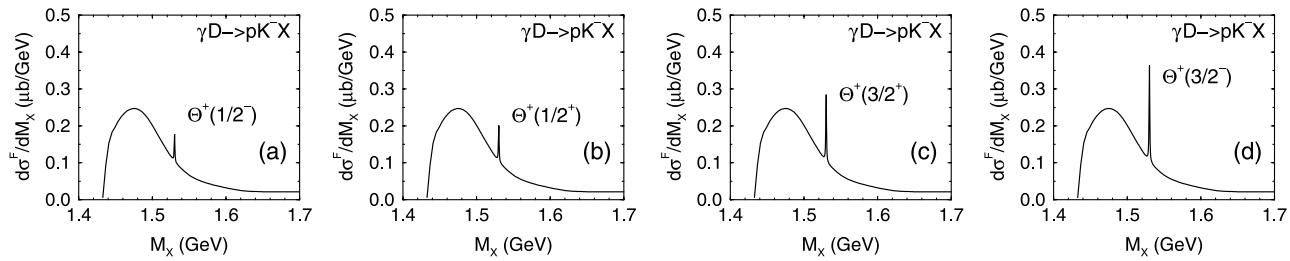

FIG. 22. Missing mass distribution in the $\gamma D \to pK^-X$ reaction at $E_\gamma = 1.7$–2.3 GeV and $M_0 = 1.52$ GeV for different Θ^+ spin and parity: (a), (b), (c) and (d) correspond to the Θ^+ spin and parity $J^P = \frac{1}{2}^-, \frac{1}{2}^+, \frac{3}{2}^+$, and $\frac{3}{2}^-$, respectively.

Finally, let us estimate the total Θ^+ formation cross section in inclusive $\gamma D \to pK^- X$ reactions with angle and ϕ-meson cuts. For $J^P_\Theta = 3/2^-$, the Θ^+ photoproduction cross section at maximum is equal to

$$\left.\frac{d\sigma^{\Theta^+ F}}{dM}\right|_{\max} \simeq 0.26\,\frac{\mu\text{b}}{\text{GeV}}, \tag{42}$$

and this value is independent of the Θ^+ decay width. Then, the total cross section for the Θ^+ signal reads

$$\sigma^{\Theta^+ F}_{\text{tot}} \simeq \frac{\pi}{2} \times \Gamma_\Theta \times \left.\frac{d\sigma^{\Theta^+ F}}{dM}\right|_{\max} \simeq 0.41\,\text{nb}. \tag{43}$$

Results for other assignments of J^P_Θ can be evaluated using Eq. (39).

B. Θ^+ formation processes in exclusive $\gamma D \to pK^- nK^+$

The reaction $\gamma D \to \Theta^+ pK^- \to npK^+K^-$ has been analyzed recently by the CLAS Collaboration [7]. We note that this experiment was designed for studying the Θ^+ photoproduction in direct $\gamma n \to \Theta^+ K^-$ elementary processes. To enforce the Θ^+ signal the data analysis was performed with some specific cuts. For convenience, we denote those cuts together with acceptance of the CLAS detector as the CLAS experimental conditions. No sizable Θ^+ signal in the nK^+ invariant mass distribution was observed. Therefore, it seems to be interesting and important to estimate the cross section for Θ^+ formation for the condition of this experiment. If we find that the formation cross section is greater than the experimental accuracy of the CLAS experiment, then it indicates problems for the Θ^+: either Θ^+ does not exist or it does exist but the Θ^+ width is much smaller than 1 MeV.

The acceptance of the CLAS detector allows to detect (i) proton and kaons with momenta greater than 0.35 and 0.25 (GeV/c), respectively; (ii) the angles of the direction of flight of the positively and negatively charged particles are greater than 9° and 15° (laboratory system), respectively. The data analysis was performed with (iii) ϕ-meson cut $M_{K^+K^-} > M_c = 1.06$ GeV, (iv) Λ^* cut $|M_{pK^-} - M_{\Lambda^*}| > \Delta_c = 25$ MeV, (v) neutron momentum cut $p_n > p_c = 0.2$ GeV/c.

The Λ^* cut almost kills the associated $\Lambda^*\Theta^+$ photoproduction shown in Fig. 1. "Almost" means that at $\Delta_c \simeq 25$–50 MeV the Λ^* signal is rather weak but finite. Nevertheless, the main contribution to the Θ^+ formation comes from the nonresonant channels shown in Fig. 12.

The neutron momentum cut strongly reduces the spectator processes, shown in Fig. 15, making rescattering channels dominant. In Fig. 24 we show the nonresonant background for nK^+ invariant mass distribution accounting for the CLAS experimental conditions. One can see the dominance of the rescattering (mainly pn rescattering) channel. Two other cuts are dangerous for the formation processes. As we have shown in Sec. IV, the dominant contribution to the Θ^+ formation comes from the forward photoproduction of a pK^- pair with $\theta_{pK^-} \lesssim 15°$ in laboratory system. In this case, the K^+ meson is a slowly moving particle. Therefore, the acceptance restriction for momentum $p_{K^+} > 0.25$ GeV/c together with

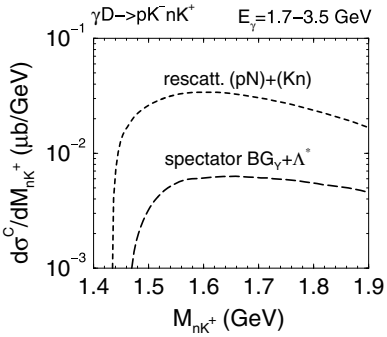

FIG. 24. The nonresonant background structure of the nK^+ invariant mass distribution in $\gamma D \to pK^- NK$ at $E_\gamma = 1.7$–3.5 GeV and for CLAS conditions.

the angle limitation for the proton and K^- meson reduce the cross section of Θ^+ formation. Note that for the inclusive photoproduction discussed above the pK^- pairs are detected in the forward direction, i.e., there are no such restrictions (cuts), and any value of p_{K^+} consistent with conservation laws is allowed.

Figure 25 shows the nK^+ invariant mass distribution in $\gamma D \to pK^- nK^+$ at $E_\gamma = 1.7$–3.5 GeV and for CLAS conditions (i)–(v). For convenience, we denote this distribution as $d\sigma^C/dM_{nK^+}$, where the superscript C indicates the CLAS conditions. One can see some Θ^+ signal against the nonresonant background dominated by the rescattering channels. We have chosen the more favorable case of $J^P_{\Theta^+} = 3/2^-$. However, even in this case the S/N ratio is about three times smaller compared to the case shown in Fig. 20(b). The Θ^+ photoproduction cross section at maximum is equal to

$$\left.\frac{d\sigma^{\Theta^+ C}}{dM}\right|_{\max} \simeq 29\,\frac{\text{nb}}{\text{GeV}}. \tag{44}$$

Using this value we can evaluate the total Θ^+ formation cross section for conditions (i)–(v)

$$\sigma^{\Theta^+ C}_{\text{tot}} \simeq 2 \times \frac{\pi}{2} \times \Gamma_{\Theta^+} \times 29\,\frac{\text{nb}}{\text{GeV}} \simeq 0.1\,\text{nb}. \tag{45}$$

In the latter case, the additional factor 2 means that only the $\Theta^+ \to nK^+$ decay channel is under consideration. Our estimate of the Θ^+ formation cross section for the CLAS

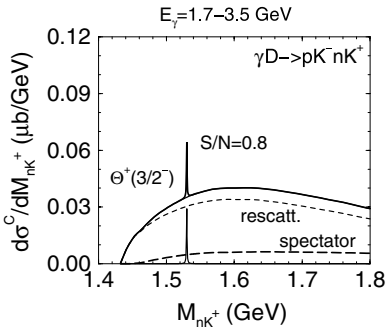

FIG. 25. The nK^+ invariant mass distribution in $\gamma D \to pK^- NK$ at $E_\gamma = 1.7$–3.5 GeV and for conditions (i)–(v).

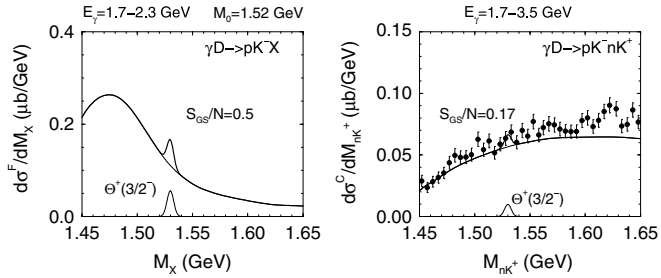

FIG. 26. (Left) Missing mass distribution in inclusive $\gamma D \to pK^- X$ at $E_\gamma = 1.7$–2.3 GeV and the pK^- photoproduction angular cut ($\theta_{pK^-} < 22^\circ$ (c.m.s.)) and ϕ-meson cut. (Right) nK^+ invariant mass distribution in exclusive $\gamma D \to pK^- nK^+$ at $E_\gamma = 1.7$–3.5 GeV and for CLAS experimental conditions (i)–(v). Experimental data from Ref. [7]. In both cases, $J^P_\Theta = 3/2^-$ and the Θ^+ signal is folded with a Gaussian resolution function with a width of 3 MeV.

experiment is three times smaller than the upper bound for the Θ^+ signal (0.3 nb) reported in Ref. [7].

For illustration, in Fig. 26 we exhibit simultaneously the missing mass distribution in the inclusive $\gamma D \to pK^- X$ reaction, averaged over the interval $E_\gamma = 1.7$–2.3 GeV with the pK^- photoproduction angular cut [$\theta_{pK^-} < 22^\circ$ (c.m. system)] (left panel) and the nK^+ invariant mass in the exclusive $\gamma D \to pK^- NK^+$ reaction for the CLAS experimental conditions (i)–(v) (right panel) together with the available experimental data [7]. Remember that the nK^+ invariant mass distribution shown in Ref. [7] is obtained after removing certain processes (contributions from ϕ meson and Λ^* excitations and the neutron spectator channels), because this experiment intends to search for direct Θ^+ production in the $\gamma n \to \Theta^+ K^-$ reaction. In our analysis of the Θ^+ formation process in the CLAS experiment we include all experimental conditions (i)–(v). To be close to the conditions of the data analysis in Ref. [7] we include in the consideration the acceptance correction factor that restores the full four-body phase space broken by the cuts (i)–(v). Our results with acceptance corrections are shown in Fig. 26.[1] The model satisfactory describes the data at low M_{nK^+} and slightly underestimates them at higher invariant mass with $M_{nK^+} > 1.6$ GeV. It is not surprising because our simple model does not pretend for detailed description of all aspects of the γD interaction in a wide interval of the photon energy. Our main purpose is the analysis of Θ^+ signal-to-noise ratio at $M_{nK^+} \sim M_\Theta$, where the model looks quite reasonable.

For the left and right panels of Fig. 26 the Θ^+ signal is folded with a Gaussian resolution function with $\sigma = 3$ MeV. Notice, that utilizing the Gaussian resolution function reduces the Θ^+ signal at the maximum position by a factor 0.21 [cf. Eq. (41)].[2] In our calculation we choose the favorable Θ^+ spin-parity $3/2^-$. The absolute value of the signal for other spin-parities decreases according to Eq. (39). From Fig. 26 (right) one can see that the effective Θ^+ signal predicted for the CLAS conditions (i)–(v) is comparable to the statistical fluctuations. Therefore, the absence of a bright Θ^+ signal in the CLAS data [7] does not exclude its possible manifestation under more favorable experimental conditions.

VII. SUMMARY

In summary, we analyzed the possible manifestation of the Θ^+ formation process in inclusive $\gamma D \to pK^- X$ reactions. If the Θ^+ exists, then in the $[\gamma D, pK^-]$ missing mass distribution there must be a distinct Θ^+ peak. Its strength depends on the Θ^+ spin and parity, and has a maximum value for $J^P_\Theta = 3/2^-$. We found that at forward angles of the pK^- pair photoproduction the signal-to-noise ratio is most favorable.

We also analyzed the recent results of the CLAS Collaboration and found that the present experimental conditions are not favorable for studying the Θ^+ formation processes. The corresponding signal-to-noise ratio is small, and the Θ^+ signal is comparable to the statistical fluctuations due to the experimental acceptance.

In our model a distinct Θ^+ signal is caused by the constructive interference of the Λ^* photoproduction from the proton and neutron in the associated $\Lambda^*\Theta^+$ photoproduction off the deuteron. In calculations we use relatively old data for Λ^* photoproduction off the proton at photon energies greater than the most favorable ones for the associated $\Lambda^*\Theta^+$ photoproduction making a corresponding extrapolation. For a more detailed study of this effect, new high-statistics low-energy data both for $\gamma p \to \Lambda^* K^+$ and $\gamma n \to \Lambda^* K^0$ are greatly desired, especially for large kaon photoproduction angles. A similar problem concerns fixing the nonresonant background. The elementary $\gamma p \to pK^+K^-$ cross section is very important here. In our analysis we used old data with low accuracy. It is clear that for understanding the Θ^+ formation processes one needs more accurate low-energy data for this elementary subprocess, too. However, our main results have a general character. Thus, it seems more reliable to detect the Θ^+ signal in the $KN \to \Theta^+$ fusion reaction realized in associated $\Lambda^*\Theta^+$ photoproduction, which may be seen in inclusive $\gamma D \to pK^- X$ reaction for certain experimental conditions.

Finally, we note that the Θ^+ formation reaction together with other accompanying processes considered in the present article may be studied experimentally at the electron and photon facilities at LEPS of SPring-8, JLab, Crystal-Barrel of ELSA, and GRAAL of ESRF.

ACKNOWLEDGMENTS

We appreciate many fruitful discussions with T. Nakano, and we thank D. Diakonov, H. Ejiri, M. Fujiwara, K. Hicks, A. Hosaka, T. Mibe, R. Mutou, M. Naruki, T. Sato, and K. Yazaki for useful comments. We appreciate B. Mecking for careful reading our manuscript and valuable suggestions. One of the authors (A.I.T.) thanks H. En'yo for offering the hospitality at RIKEN. This work was supported by BMBF grant 06DR121, GSI-FE.

[1] The acceptance correction increases the total cross section in Eq. (45) to 0.15 nb.

[2] Our choice $\sigma = 3$ MeV is rather illustrative. Using Eq. (41) one can easily reestimate the amplitude of the Θ^+ signal for any value of σ.

APPENDIX A: KINEMATICS FOR THE REACTION $\gamma D \to pK^- NK$

Let us consider the determination of the momenta of all outgoing particles in the $\gamma D \to pK^- NK$ reaction at fixed input parameters defined in Sec. II in detail. The square of the total energy in the c.m. system is

$$s_D = M_D^2 + 2M_D E_\gamma, \tag{A1}$$

where M_D is the deuteron mass and E_γ is the photon energy in the laboratory system. The momenta p_i and p_f read

$$\begin{aligned} p_i &= \frac{\sqrt{\lambda(s_D, M_D^2, 0)}}{2\sqrt{s_D}} = \frac{s_D - M_D^2}{2\sqrt{s_D}}, \\ p_f &= \frac{\sqrt{\lambda(s_D, M_X^2, M_Y^2)}}{2\sqrt{s_D}}, \end{aligned} \tag{A2}$$

where $\lambda(x^2, y^2, z^2) = [x^2 - (y-z)^2][x^2 - (y+z)^2]$ is the triangle kinematical function. The four-momenta of proton and K^- meson in the Y rest frame is defined by the mass M_Y and the solid angle Ω_Y. Thus, the absolute value of the decay three-momentum reads

$$\tilde{\bar{q}} = \frac{\sqrt{\lambda(M_Y^2, M_K^2, M_N^2)}}{2M_Y}. \tag{A3}$$

Then the four-momenta are defined as

$$\begin{aligned} \tilde{p}_{K^-} &= (\tilde{E}_{K^-}, \tilde{\bar{q}} \sin\theta_Y \cos\varphi_Y, \tilde{\bar{q}} \sin\theta_Y \sin\varphi_Y, \tilde{\bar{q}} \cos\theta_Y), \\ \tilde{E}_{K^-} &= \sqrt{\tilde{\bar{q}}^2 + M_K^2} \end{aligned} \tag{A4}$$

and

$$\begin{aligned} \tilde{p}_p &= (\tilde{E}_p, -\tilde{\bar{q}} \sin\theta_Y \cos\varphi_Y, -\tilde{\bar{q}} \sin\theta_Y \sin\varphi_Y, -\tilde{\bar{q}} \cos\theta_Y), \\ \tilde{E}_p &= \sqrt{\tilde{\bar{q}}^2 + M_N^2}, \end{aligned} \tag{A5}$$

respectively. Note, that here the $\tilde{\mathbf{z}}$ axis is taken along $\mathbf{p}_Y$, and the $\tilde{\mathbf{y}}$ axis coincides with $\mathbf{y}$. Next, we boost these momenta to the c.m. system along the $\tilde{\mathbf{z}}$ axis as

$$\begin{aligned} p'_{p0} &= \gamma_Y(\tilde{p}_{p0} + v_Y \tilde{p}_{p3}), \quad p'_{p3} = \gamma_Y(\tilde{p}_{p3} + v_Y \tilde{p}_{p0}), \\ p'_{p1} &= \tilde{p}_{p1} \quad p'_{p2} = \tilde{p}_{p2}, \end{aligned} \tag{A6}$$

where $v_X = p_f/\sqrt{p_f + M_X^2}$ and $\gamma_X = v_X/\sqrt{1 - v_X^2}$. Then, we rotate the coordinate system around the $\mathbf{y}$ axis by the angle θ to get the momenta in the c.m. system with $\mathbf{z}$ along the photon momentum $\mathbf{k}$

$$\begin{aligned} p_{p1} &= p'_{p1} \cos\theta + p'_{p3} \sin\theta, \\ p_{p3} &= p'_{p3} \cos\theta - p'_{p1} \sin\theta, \\ p_{p2} &= p'_{p2}, \quad p_{p0} = p_{p0}'. \end{aligned} \tag{A7}$$

Similarly, we transform the momenta of the outgoing nucleon N and K meson of the X system with obvious substitutions: $M_Y \to M_X, \theta_Y \to \theta_X, \varphi_Y \to \varphi_X$, and $\theta \to \pi + \theta$.

APPENDIX B: AMPLITUDES OF THE ELASTIC-SCATTERING PROCESSES

A. $K^- N \to K^- N$ scattering

Let us consider the elastic $K^- p \to K^- p$ scattering. The amplitude is related to the differential cross section via

$$\frac{d\sigma^{Kp}}{d\Omega} = \frac{1}{64\pi^2 s} \frac{p_f}{p_i} \frac{1}{2} \sum_{m_i m_f} |T^{Kp}_{m_f m_i}(s, \cos\theta)|^2, \tag{B1}$$

where p_i, m_i and p_f, m_f are the three-dimensional relative momenta and the proton spin projections in the initial and the final states, respectively; s is the square of the total energy in the c.m. system; and θ denotes the scattering angle. In our calculations we take the differential cross section from experiment [33], given as a function of the scattering angle in certain energy intervals. In rescattering processes, one of the incoming proton may be off-shell, and therefore, generally, $p_i \neq p_f$. Thus, the scattering angle is defined as

$$\cos\theta = \frac{2E_i E_f - 2M_K^2 + t}{p_i p_f} \tag{B2}$$

with t, $p_{i(f)}$ and $E_{i(f)}$ given as

$$\begin{aligned} t &= (q - q')^2, \\ |p_i| &= \frac{\sqrt{\lambda(s, M_K^2, \bar{M}_N^2)}}{2\sqrt{s}}, \\ |p_f| &= \frac{\sqrt{\lambda(s, M_K^2, M_N^2)}}{2\sqrt{s}}, \\ E_{i(f)} &= \sqrt{\mathbf{p}^2_{i(f)} + M_K^2}, \end{aligned} \tag{B3}$$

where q and q' are the kaon four-momenta in initial and final states, respectively, and $\bar{M}_N^2$ is the square of the four-momentum of the incoming off-shell nucleon.

We use the following parametrization of the differential cross section (in mb)

$$\begin{aligned} p_L < 0.3663, &\quad d\sigma^{Kp}/d\Omega = 3.01(2 + \cos\theta)/s, \\ 0.3663 < p_L < 0.4185, &\quad d\sigma^{Kp}/d\Omega = 3.01(1 + 3\cos^2\theta)/s, \\ 0.4185 < p_L, &\quad d\sigma^{Kp}/d\Omega = 0.5[1 + (1 + \cos\theta)^\delta], \end{aligned} \tag{B4}$$

where p_L is the kaon momentum in laboratory frame in GeV/c and

$$\delta = 1.443 \ln(13.33 p_L - 1). \tag{B5}$$

The spin dependence of the amplitude is chosen in the simplest form as

$$T^{Kp}_{m_f m_i} = T_0(\delta_{m_i, m_f} + \delta_{-m_i, m_f}). \tag{B6}$$

TABLE I. Parameters of the function $d\sigma/dt = Ae^{Bt_a+Ct_a^2}$.

p_L (MeV/c)	A [mb/(GeV/c)^2]	B (GeV/c)$^{-2}$	c (GeV/c)$^{-4}$
<899	87.1	0.96	2.91
900–999	78.8	1.17	1.89
1000–1099	64.7	1.00	0.72
1100–1199	60.4	2.01	2.10
1200–1299	79.6	4.38	3.96
1300–1399	107.4	5.76	3.68
1400–1499	116.1	5.45	2.04
1500–1599	126.2	6.51	3.56
1600–1699	137.0	7.20	3.80
1700–1799	140.9	7.66	4.39
1800–2399	141	7.66	3.55

Concerning the K^-n reaction, we employ $d\sigma^{K^-n\to K^-n} \simeq d\sigma^{K^-p\to K^-p}$.

B. $pN \to pN$ scattering

For the differential cross section of the elastic pp scattering we use the parametrization of Ref. [34]:

$$\frac{d\sigma}{dt} = A\exp\left(Bt_a + Ct_a^2\right), \tag{B7}$$

TABLE II. Parameters of the function $d\sigma/dt = A[(1-\alpha)e^{Bt_a} + \alpha\, e^{Ct_a}]$.

p_L (MeV/c)	α	B (GeV/c)$^{-2}$	c (GeV/c)$^{-2}$
2200–2599	0.022	7.8	0.7
2600–2999	0.015	8.0	0.7
3000–3500	0.015	8.8	1.0

where $t_a = 2M_N^2 - 2E^2 + 2p^2|\cos\theta|$, p and E are the proton momentum and energy in the c.m. system, respectively. The parameters A, B, and C are listed in Table I. Here p_L is the proton momentum in laboratory system.

For $p_L = 2.2$–3.5 GeV/c the cross section is parametrized as a sum of two exponentials

$$\frac{d\sigma}{dt} = A[(1-\alpha)\exp(Bt_a) + \alpha\exp(Ct_a)], \tag{B8}$$

where $A \simeq 141$ mb/GeV^2 and α, B, and C are listed in Table II.

Similarly to the K^-p scattering we ignore the spin dependence of the amplitude. In our study we assume approximately $d\sigma^{pn} \simeq d\sigma^{pp}$.

[1] T. Nakano *et al.* (LEPS Collaboration), Phys. Rev. Lett. **91**, 012002 (2003).

[2] V. V. Barmin *et al.* (DIANA Collaboration), Phys. At. Nucl. **66**, 1715 (2003); S. Stepanyan *et al.* (CLAS Collaboration), Phys. Rev. Lett. **91**, 252001 (2003); V. Kubarovsky *et al.* (CLAS Collaboration), *ibid.* **92**, 032001 (2004); **92**, 049902(E) (2004); J. Barth *et al.* (SAPHIR Collaboration), Phys. Lett. **B572**, 127 (2003); A. E. Asratyan, A. G. Dolgolenko, and M. A. Kubantsev, Phys. At. Nucl. **67**, 682 (2004); A. Airapetian *et al.* (HERMES Collaboration), Phys. Lett. **B585**, 213 (2004); S. Chekanov *et al.* (ZEUS Collaboration), *ibid.* **B591**, 7 (2004); M. Abdel-Bary *et al.* (COSY-TOF Collaboration), *ibid.* **B595**, 127 (2004); A. Aleev *et al.* (SVD Collaboration), Phys. At. Nucl. **68**, 974 (2005).

[3] K. Hicks, Prog. Part. Nucl. Phys. **55**, 647 (2005).

[4] V. D. Burkert, Int. J. Mod. Phys. A **21**, 1764 (2006); R. A. Schumacher, AIP Conf. Proc. **842**, 409 (2006); arXiv:nucl-ex/0512042.

[5] M. Danilov, in *Proceedings of the Les Rencontres de Physique de la Valleè d'Aoste-Results and Perspectives in Particle Physics*, La Thuile, Aosta Valley, 2005. edited by M. Greco Frascati Physics Series, Vol. XXXIX-Special Issue, p. 193; arXiv:hep-ex/0509012.

[6] A. I. Titov, A. Hosaka, S. Daté, and Y. Ohashi, Phys. Rev. C **70**, 042202(R) (2004).

[7] B. McKinnon *et al.* (The CLAS Collaboration), Phys. Rev. Lett. **96**, 212001 (2006).

[8] M. Batarelli *et al.* (The CLAS Collaboration), Phys. Rev. Lett. **96**, 042001 (2006); R. De Vita *et al.* (The CLAS Collaboration), Phys. Rev. D **74**, 032001 (2006).

[9] V. V. Barmin *et al.* (DIANA Collaboration), arXiv:hep-ex/0603017.

[10] K. Miwa *et al.* (KEK-PS E522 Collaboration), Phys. Lett. **B635**, 72 (2006).

[11] Y. Oh, K. Nakayama, and T.-S. Lee, Phys. Rep. **423**, 49 (2006).

[12] T. Hyodo, S. Sarkar, A. Hosaka, and E. Oset, Phys. Rev. C **73**, 035209 (2006).

[13] A. I. Titov, B. Kämpfer, S. Daté, and Y. Ohashi, Phys. Rev. C **72**, 035206 (2005).

[14] D. P. Barber *et al.* (LAMP2 Group), Z. Phys. C **7**, 17 (1980).

[15] A. Sibirtsev, J. Haidenbauer, S. Krewald, U-G. Meissner, and A. W. Thomas, arXiv:hep-ph/0509145.

[16] N. Muramatsu *et al.* (LEPS Collaboration), in *Proceedings of the 14th International Workshop on Deep Inelastic Scattering, Tsukuba, Japan, 2006*, edited by M. Kuze *et al.*, (World Scientific Publishing Co., Singapore) to be published; http://www-conf.kek.jp/dis06/program-wg5.htm.

[17] S. I. Nam, A. Hosaka, and H. C. Kim, Phys. Rev. D **71**, 114012 (2005).

[18] A. I. Titov, H. Ejiri, H. Haberzettl, and K. Nakayama, Phys. Rev. C **71**, 035203 (2005).

[19] H. J. Besch, G. Hartmann, R. Kose, F. Krautschneider, W. Paul, and U. Trinks, Nucl. Phys. **B70**, 257 (1974).

[20] J. Barth *et al.* (SAPHIR Collaboration), Eur. Phys. J. A **17**, 269 (2003).

[21] T. Mibe *et al.* (LEPS Collaboration), Phys. Rev. Lett. **95**, 182001 (2005).

[22] E. Anciant *et al.* (The CLAS Collaboration), Phys. Rev. Lett. **85**, 4682 (2000).

[23] R. Erbe *et al.* (Aachen-Berlin-Bonn-Hamburg-Heidelberg-Muenchen Collaboration), Phys. Rev. **188**, 2060 (1969).

[24] W. Roberts, Phys. Rev. C **70**, 065201 (2004).
[25] S. Eidelman *et al*. (Particle Data Group), Phys. Lett. **B592**, 1 (2004).
[26] R. A. Arndt, I. I. Strakovsky, and R. L. Workman, Phys. Rev. C **68**, 042201(R) (2003) [Erratum-*ibid*. **69**, 019901(E) (2004)]; J. Haidenbauer and G. Krein, Phys. Rev. C **68**, 052201(R) (2003); A. Sibirtsev, J. Haidenbauer, S. Krewald, and U-G. Meissner, Phys. Lett. **B599**, 230 (2004); A. Sibirtsev, J. Haidenbauer, S. Krewald, and U-G. Meissner, Eur. Phys. J. A **23**, 491 (2005); A. Casher and S. Nussinov, Phys. Lett. **B578**, 124 (2004).
[27] V. Guzey, Phys. Rev. C **69**, 065203 (2004).
[28] M. E. Peskin and D. V. Schroeder, *An Introduction to Quantum Field Theory* (Addison-Wesley, Reading, MA, 1996).
[29] S. Capstick, P. R. Page, and W. Roberts, Phys. Lett. **B570**, 185 (2003).
[30] R. L. Jaffe and A. Jain, Phys. Rev. D **71**, 034012 (2005).
[31] T. Hyodo and A. Hosaka, Phys. Rev. D **71**, 054017 (2005).
[32] T. Nishikawa, Y. Kanada-En'yo, O. Morimatsu, and Y. Kondo, Phys. Rev. D **71**, 076004 (2005).
[33] C. J. Adams *et al*., Nucl. Phys. **B96**, 54 (1975).
[34] B. A. Ryan, A. Kanofsky, T. J. Devlin, R. E. Mischke, and P. F. Shepard, Phys. Rev. D **3**, 1 (1971).